A data analysis to bed dynamics in the Western Scheldt estuary

Morphological parameter estimation and deformation analysis near the shoal of Walsoorden

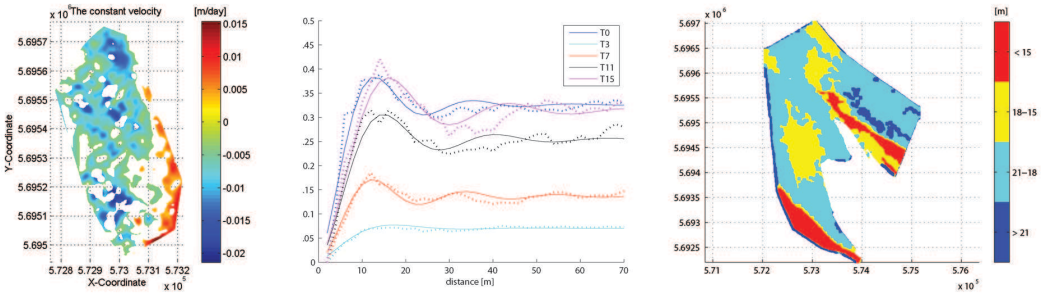

Master Thesis
Geomatics

S.J.A. Pluymaekers

May 2007

Section Mathematical Geodesy and Positioning
Delft Insitute of Earth Observation and Space Systems (DEOS)
Faculty of Aerospace Engineering
Delft University of Technology

Graduation professor:	Prof. dr. D.G. Simons (TU Delft)
Supervisor:	Dr. R.C. Lindenbergh (TU Delft)
Co-reader:	Ir. J.G. De Ronde (RIKZ)

Preface

This thesis is the result of six and a half years education in the field of Geodesy. In those years I had the pleasure to learn the principles of surveying, to absorb magnificent information about land management, photogrammetry and gravitational fields and to discover the beautiful realm of the mathematical geodesy. This education enabled me to develop myself significantly. However, as a firm believer in *éducation permanente*, I am very aware of the fact that I still have a lot to learn.

I can only hope that during my further education, I will get as much support as I received from the teachers at the Delft University of Technology. A special word of appreciation to two persons from the section Mathematical Geodesy and Positioning, which supported me with my thesis, prof. dr. D.G. Simons and dr. R.C. Lindenbergh. I would like to thank professor Simons for being very interested in my research and giving me valuable tips and comments. Roderik Lindenbergh, thank you very much for all the advises, interest, discussions and support during my graduation project.

However, the persons to whom I owe the greatest gratitude are my family. They taught me a lot more than any institution could ever do. Especially I would like to thank my parents, who imparted to me the value and beauty of education. Their constant interest, support and encouragement did not decline with a separation distance of about 8000 kilometers during a large part of my study.

Steven Pluymaekers
May 2007

Summary

The Western Scheldt estuary is the entrance to one of the major harbours in the world, the port of Antwerp. It is important to keep this harbour accessible for ever growing ships, which unavoidable leads to dredging activities. On the other hand, this estuary forms the basis of a unique ecosystem, which needs to be protected. In order to combine these at fist sight contradicting objectives, a new idea of morphological management, including well considered dredging and disposal activities, is proposed.

As a pilot project 500.000 m^3 of dredged material is disposed near the shoal of Walsoorden. A morphological monitoring program of the sand dump is performed, resulting in a time series of multi-beam echo sounding data. This data enables us to get insight in the Western Scheldt bed from a data point of view. This estuary bed has a complex morpho-dynamic structure, containing subaqueous bed forms (called sand dunes or sand waves) of different size.

In this study, a method is introduced and tested to analyze changes in depth and subaqueous dune parameter values. Periodic bed forms are first separated from the 'global topography' in a filtering procedure. Then dune parameter class maps are determined from the bed form component of the data. These division in classes enables a segmentation of the area in regions with similar morphological behaviour. Subsequently, two of those regions are analyzed over time. For this task, the disposal location near the shoal of Walsoorden with its direct neighbourhood and a more stable area further north of the shoal of Walsoorden are chosen.

In these areas changes in the 'global topography' are analyzed using the method of deformation analysis, while the sand dune parameters are obtained using morphological parameter estimation. In the deformation analysis procedure, that mathematical model is selected, which describes best the changes in a time series of filtered observations. Models of stability, local constant velocity and local constant acceleration are considered. For the analysis of the morphological parameters, two different estimation methods are used. A first method based on *directional variograms* is compared with the second, rather simple technique, which makes use of *profile lines*.

Most of the points at the dump location follow the hypothesis of constant negative velocity, indicating a deposition of a part of the dumped material. The sand is redistributed in the south east direction toward the shoal of Walsoorden. The different estimation methods for the morphological changes of the subaqueous sand dunes work rather well. They give in general the same results, which gives confidence in the outcome. The amplitude gradually recovers until the original level is reached again after approximately three months. The wave length behaves differently: both methods indicate an increase in this parameter value.

The points analyzed in the more stable area showed a sudden deformation in the eastern part, possibly caused by sand dumping. For the stable points, the parameter values are calculated which show a slowly change over time. An amplitude outlier is found in the third sounding moment, but an explanation for this phenomenon is not yet known.

A first attempt to link the changes of the parameter values to changing weather conditions or the tidal data was not successful. Neither visual inspection, nor the techniques of principal component analysis or correlation coefficients calculation show a clear linear relation. However, a rather weak correlation is found between the wave length and the amplitude values, there may be a relation but it is not totally clear if this is really the case.

Samenvatting

Het Westerschelde estuarium vormt de toegangspoort tot een van de grootste havens ter wereld, de haven van Antwerpen. Het is van belang deze haven toegankelijk te houden voor de steeds groter wordende schepen. Dit heeft als gevolg dat er bagger activiteiten moeten plaatsvinden. Aan de andere kant is dit estuarium de basis voor een uniek ecosysteem, dat bescherming nodig heeft. Om deze twee op het oog tegengestelde belangen te kunnen verenigen, is er een nieuwe morfologische management strategie voorgesteld. Een onderdeel hiervan is een weloverwogen keuze van bagger- en dumplocaties.

Voor een proefproject is 500.00 m^3 baggermateriaal gestort bij de plaat van Walsoorden. Vervolgens is een morfologisch monitoring programma uitgevoerd, waarin een deel van de Westerschelde bodem tweewekelijks is opgemeten. Deze unieke multi-beam echo sounding dataset stelt ons in staat om vanuit het perspectief van de data inzicht te krijgen in de Westerschelde bodem. Deze bodem heeft een complexe morfo-dynamische structuur, waarin regelmatige bodemvormen (zandgolven of zandduinen) van verschillende grootte voorkomen.

In dit onderzoek is een methode ontwikkeld en getest om de veranderingen in de diepte en de veranderingen in de parameterwaarden van de zandduinen te analyseren. De regelmatige bodemvormen zijn eerst gescheiden van de 'globale topografie' door middel van een filter procedure. Vervolgens zijn de duin parameters geclassificeerd en gesegmenteerd in gebieden met een vergelijkbaar morfologisch gedrag. Van twee van deze gebieden is het gedrag door de tijd geanalyseerd. De stortlocatie met haar directe omgeving en een stabieler gebied verder ten noorden van de plaat van Walsoorden zijn hiervoor gekozen.

In deze gebieden zijn de veranderingen in de 'globale topografie' gedetecteerd met behulp van deformatie analyse, terwijl de zandduin parameters verkregen worden door morfologische parameter schatting. In de deformatie procedure wordt het mathematisch model gekozen dat de veranderingen in de tijd op de beste manier beschrijft. In dit onderzoek zijn de stabiliteitsmodellen, constante snelheidsmodellen en constante versnellingsmodellen overwogen. Voor de analyse van de morfologische parameters zijn twee verschillende schatting-methodes gebruikt. De eerste methode, gebaseerd op *richtingsafhankelijke variogrammen* wordt vergeleken met de tweede, vrij eenvoudige methode die gebruik maakt van *profiellijnen*.

De meeste punten van de stortlocatie volgen de hypothese van constante negatieve snelheid. Dit impliceert erosie van een deel van het gestorte materiaal. Het zand dat geërodeerd is kan zuid oostelijk van de stortlocatie worden teruggevonden in de richting van de plaat van Walsoorden. Bij de schatting van de morfologische parameters zijn voor beide methodes over het algemeen de resultaten hetzelfde, hetgeen vertrouwen geeft in de uitkomst. De amplitude herstelt zich na de zandstort, totdat de originele waarde van voor de dump bereikt is na ongeveer

drie maanden. De golflengte gedraagt zich anders; de twee methodes geven een stijging aan van deze parameter waarde.

Het tweede gebied vertoont een plotselinge deformatie in het oostelijke gedeelte, mogelijk veroorzaakt door een zandstort. Voor de stabiele punten zijn de parameter waarden van de zandduinen berekend. Zij stijgen licht in de tijd. Een plotselinge afname in de amplitude is gevonden in de derde opname, maar een verklaring voor dit fenomeen is nog onbekend.

Een eerste poging om de veranderingen in de parameter waarden te koppelen aan veranderende weersomstandigheden en getijde data was niet succesvol. Noch visuele inspectie, noch de technieken van principal component analysis of correlatie coefficienten impliceren een lineaire relatie. Wel is een, enigzins zwakke, correlatie gevonden tussen de golflengte en amplitude waarden. Het is zeer wel mogelijk dat er een relatie is, maar gezien de matige sterkte kan dat niet met zekerheid gezegd worden.

Contents

Chapter 1

Introduction

The Western Scheldt estuary is the entrance to one of the major harbours in the world, the port of Antwerp. It is important to keep this harbour accessible for ever growing ships, which unavoidable leads to dredging activities. On the other hand this estuary, with its multi-channel system, forms the basis of a unique ecosystem, which is highly valuable and therefore needs to be protected.

In 1999 the governments of Flanders and the Netherlands agreed to cooperate closer and laid down a strategy, the 'Long Term Vision' (LTV), in which they expressed how to manage the Scheldt estuary with special attention for safety against flooding, accessibility of the ports and the maintenance of the nature values. One of the main targets was the preservation of the multi-channel system. In order to reach these objectives the Port of Antwerp Expert Team (PAET) proposed the idea of morphological management, which includes well considered dredging and disposal activities, but also adaptations of the hard bordering to modify the erosion-transport-deposition process [12].

A first test of this new strategy was performed near the shoal of Walsoorden (Figure 1.1). The disposal of dredged material near the seaward tip of this shoal should reinforce the multi-channel system and improve the self-erosive capacity of the flow. To investigate the effects of this approach 500.000 m^3 of sand was dumped and consecutively the area was extensively monitored at a two week interval. This has resulted in a time series of multi-beam echo sounding (MBES) data and as the exact sounding days are known, the weather conditions and tidal water level data during the monitoring period can be found easily. This information can be used to investigate changes near the shoal of Walsoorden and analyze the influence of the weather conditions and tides.

The objective of this research is *to get insight in the complex morpho-dynamic behaviour of the Western Scheldt bed from a data point of view, using the two weekly MBES surveying.*

In order to reach this goal, three questions need to be answered:

1. *How does the Western Scheldt bed change over time?*
   In answering this question the erosion of the sand dump will be considered including the consecutive distribution of the disposed sand elsewhere. Also the dynamics of an area in the Scheldt estuary without sand dump will be analyzed.

2. *How do morphological parameter values change over time?*

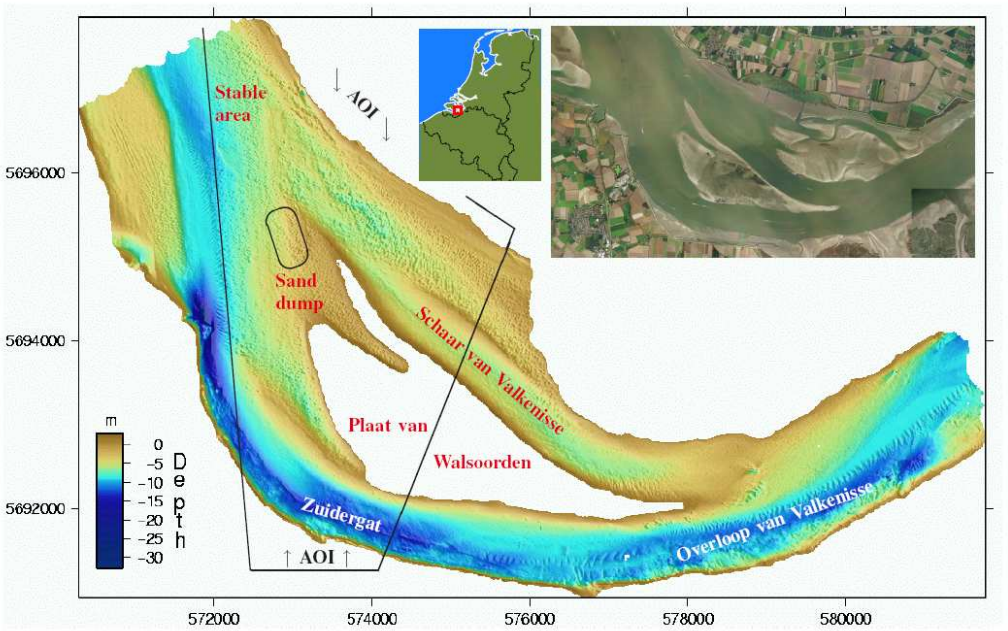

Figure 1.1: The area of interest (AOI) near the shoal of Walsoorden (In Dutch: Plaat van Walsoorden).

The Western Scheldt bed is covered with specific bed forms, usually called sand waves or sand dunes. In this second question three parameters of these bed forms, the orientation, the height and the length, will be investigated. Of special interest is the development of the parameters over time. The reappearance speed of sand waves on the dump location will also be discussed.

3. *Is there a relation between the morphological changes in the Western Scheldt bed and the weather or water level conditions?*
   The exact sounding days are known. Therefore it is possible to obtain the weather conditions and the tidal water level information in between the soundings. This last question deals with a possible correlation between these meteorological and tidal datasets and the results obtained in answering question 2.

Answers to this questions are found by combining several techniques. Signal decomposition is performed to separate large scale topography from different scales of bed forms in order to perform a more reliable parameter value estimation. A segmentation step is proposed to distinguish between different deformation regimes at locations with different characteristics in topography and bed form parameters, while deformation in homogeneous areas is traced by applying the Delft method of deformation analysis, which compares different deformation scenarios in a data snooping procedure, while incorporating the uncertainty and correlation in the input data. The deformation scenarios tested include estuary bottom stability, local constant velocity and local constant acceleration.

The methodology is applied in two different cases. First for the detection and analysis of the sand dump area, where strong changes are expected. Second, a homogeneous and probably more stable region is selected by means of the classification procedure. For both areas the deformation

and the development of the sand dune parameters over time is inspected. However, by classifying the whole area of interest, the total overview will not be ignored. Using this combination of techniques provides a way of ordering the complex morpho-dynamics in the Western Scheldt multi-channel system.

First, background information on the multi-beam echo sounder and the Western Scheldt morphology is given in Chapter 2. Chapter 3 gives insight in the methods used for change detection, which includes data decomposition (filtering), morphological parameter estimation and deformation analysis. In Chapter 4 the classification of the total study area will be discussed, whereas Chapter 5 deals with the first area, the dump location. Chapter 6 focuses on a second more stable area in the Scheldt estuary and Chapter 7 gives insight in the correlation between dune parameters, the weather conditions and the tidal data. Finally, this thesis will be completed with the conclusions and recommendations described in Chapter 8.

Chapter 2

Estuary floor mapping

In this chapter an introduction to the mapping of the Western Scheldt estuary is given. First, the echo sounding techniques are described in Section 2.1. Section 2.2 focuses on the Western Scheldt morphology, including dominating currents and specific bed forms. Finally, this chapter will end with a brief description of the data sets used in this study (Section 2.3).

2.1 Echo sounding

In the beginning of the 20th century the technique of active acoustic systems was developed. It was a great improvement for the bathymetric maps, which are necessary for safe navigation. Realizing that almost 70 % of the earth surface is covered with water, this technique opens a complete new world. Nowadays the applications of underwater acoustics are widespread: navigation, sea floor mapping and military purposes are just the most important and widely known.

One can make a distinction between *active* and *passive* acoustic systems. The first one transmits a characteristic signal and receives it after the reflection, while the latter intercepts and exploits the signals coming from the object itself. These systems for the detection of targets are usually called *Sonars*, which is an acronym for *Sound Navigation and Ranging* [15].

2.1.1 Principles of echo sounding

The most common underwater acoustic system is the echo sounder, suitable for navigation and mapping. Active acoustic mapping systems determine the depth from the observation of the travel time of acoustic waves. A pulse is transmitted from a vessel and after traveling through the water it is reflected by the bottom, back to the hydrophone. The depth can easily be obtained from:

$$D = \frac{c \cdot \Delta T}{2} \tag{2.1}$$

with D the depth, c the sound speed in water and ΔT the two way travel-time.

Figure 2.1 demonstrates the components of a basic echo sounder[2]:

- A transmitter, which generates the pulses
- A transmitter/receiver switch, which passes the power to the transducer
- A transducer, which converts the electrical power into the acoustic power, sends the acoustic signal into the water, receives the echo and converts it into an electrical signal

- A receiver, which amplifies the echo signal and sends it to the recording system
- A recorder, which controls the signal emission, measures the travel time of the acoustic signal, stores the data and converts time intervals into ranges

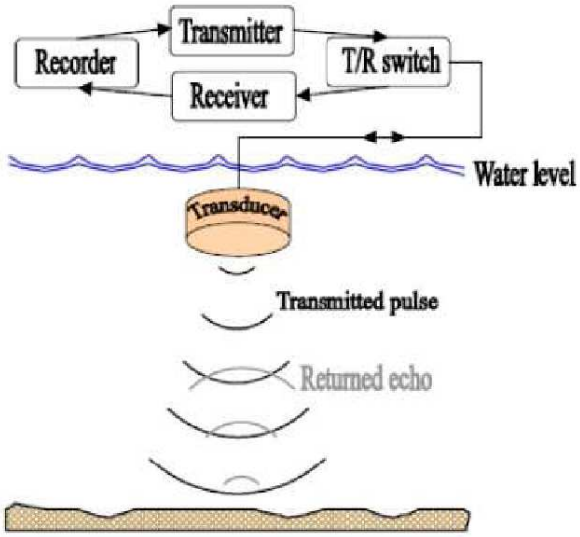

Figure 2.1: The echo sounding principle. Source: [6].

This principle is used in most sea floor mapping systems and can be found in the following devices [15] (also shown in Figure 2.2):

- Single-beam echo sounders, in use since the 1920s, measuring depths directly vertical of a ship
- Side-scan sonars, in use since the 1960s, providing acoustic images of the sea floor from echoes at grazing angles of incidence
- Multi-beam echo sounders, in use since the late 1970s, performing a large number of measurement from one signal

Today's sea floor mapping is dominated by multi-beam echo sounders. These sonar systems can, after transmission of a single signal, perform a large number of point measurements on a wide strip of terrain perpendicular to the ship's route and are therefore very suitable for bathymetric measurements.

2.1.2 The multi-beam echo sounder

The multi-beam echo sounders are extensions and improvements of the older single-beam echo sounders, and are able to cover the bottom rapidly and accurately. These systems transmit and receive a fan of beams with small individual widths across the axis of the ship. Thus, for one measurement by a multi-beam sounder, a lot of time and angle couples can be obtained. Using this principle, each pulse transmission generates a high number of depth soundings.

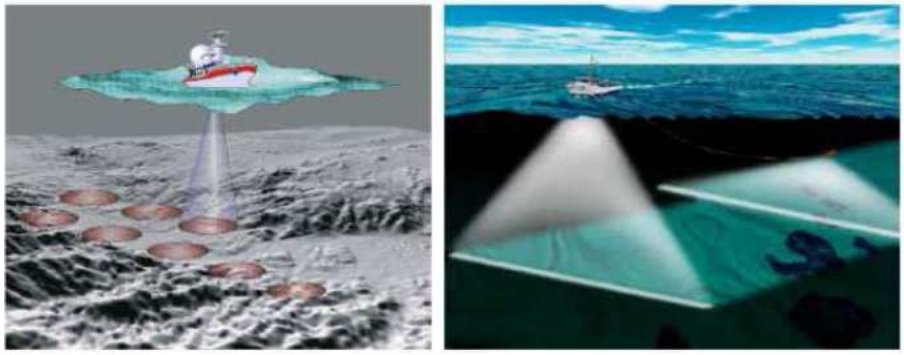

Figure 2.2: Echo sounding systems. On the left: Single-beam echo sounding. On the right: Multi-beam echo sounding and a side-scan sonar mounted on a towfish, behind the vessel. Source: [16].

If we assume that the sound velocity profile is constant and the acoustic paths are rectilinear, the across-track position y and the depth D shown in Figure 2.3, can easily be calculated:

$$y = \frac{c \cdot \Delta T}{2} \sin \psi \tag{2.2}$$

$$D = \frac{c \cdot \Delta T}{2} \cos \psi \tag{2.3}$$

with ψ the angle between the vertical and actual beam direction. Hence, the basic principle as stated in Eq. 2.1 is extended with the beam angle for the multi-beam system.

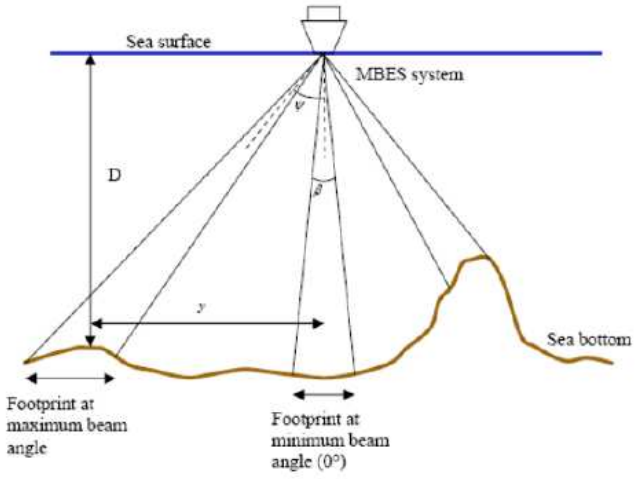

Figure 2.3: The multi-beam echo sounder. Source:[2].

The coordinates calculated with Eq. 2.2 and Eq. 2.3 are not absolute, but relative to the position of the echo sounder. In order to locate these measurements accurately one needs several ancillary systems. A positioning system is used to determine the location of the ship and an attitude sensor is essential for the compensation of roll, pitch and yaw. Furthermore, one preferably

needs sound velocity profiles to correct the acoustic paths and sound velocity measurements to improve the beam forming.

There are three main types of errors using acoustic echo sounding techniques [15]:

- Errors in the acoustic measurements itself, depending on the Signal to Noise Ratio (SNR)
- Movements of the support platform, like roll, pitch, yaw and heave
- Inaccuracies in sound velocity corrections, modifying the acoustic paths

To minimize the second problem, one can make use of an attitude sensor, which constantly measures the angular position of the sonar. The last error type can be reduced by using local sound velocity profiles, measured directly or extracted from geographical databases.

2.2 Western Scheldt morphology

The present Scheldt river has a length of approximately 350 km and originates in Gouy (Fr). It flows through France, Belgium and the Netherlands toward the North Sea. The Scheldt estuary, defined as that part of the river basin with a tidal influence, has a length of about 200 km and begins in Gent (B)(Figure 2.4). Its cross-sectional area decreases exponentially from the estuary mouth to the estuary head. The width-averaged depth decreases from some 15 meters at Vlissingen to only 3 meters at the estuary head near Gent. The width reduces from about 6 kilometers at the estuary mouth, via some 2-3 kilometers near Bath, to less than 100 meters near Gent. Morphologically, it can be divided in three distinct zones [8]:

1. An extensive sub tidal delta bisected by two large channels, seaward of Vlissingen
2. A multiple channel system separated by elongated shoals in the seaward marine part of the estuary between Vlissingen and Doel, the Western Scheldt. The elongated (inter)tidal shoals are characteristic for the tide dominated estuaries.
3. A single tidal channel with alternate bank-attached bars landward of Doel.

In this thesis a part of the multiple channel system (zone 2) is investigated.

2.2.1 Channels

The Western Scheldt consists of a system of tidal channels. The channel system shows a regular, repetitive pattern of ebb and flood channels. The larger main ebb channels form a more or less continuously meandering channel between Belgium and the estuary mouth. The main flood channels originate in the bends of the ebb channels and are generally shallower. In general, the shallow parts are mainly found at the seaward end of the ebb channels and at the landward end of the flood channels. Connections between those main ebb and flood channels are sometimes made by some small channels. Hence, the channel types in the Scheldt estuary can be characterized as follows [8]:

1. *Main channels.* They are the largest channels and transport most of the total tidal discharge. In the Western Scheldt two large main channels can be identified that occur side by side: a curved main ebb channel and a straight main flood channel. Also some smaller, former main channels exists. They are separated from the neighbouring large main channels by inter-tidal shoals. Their transport function is limited.

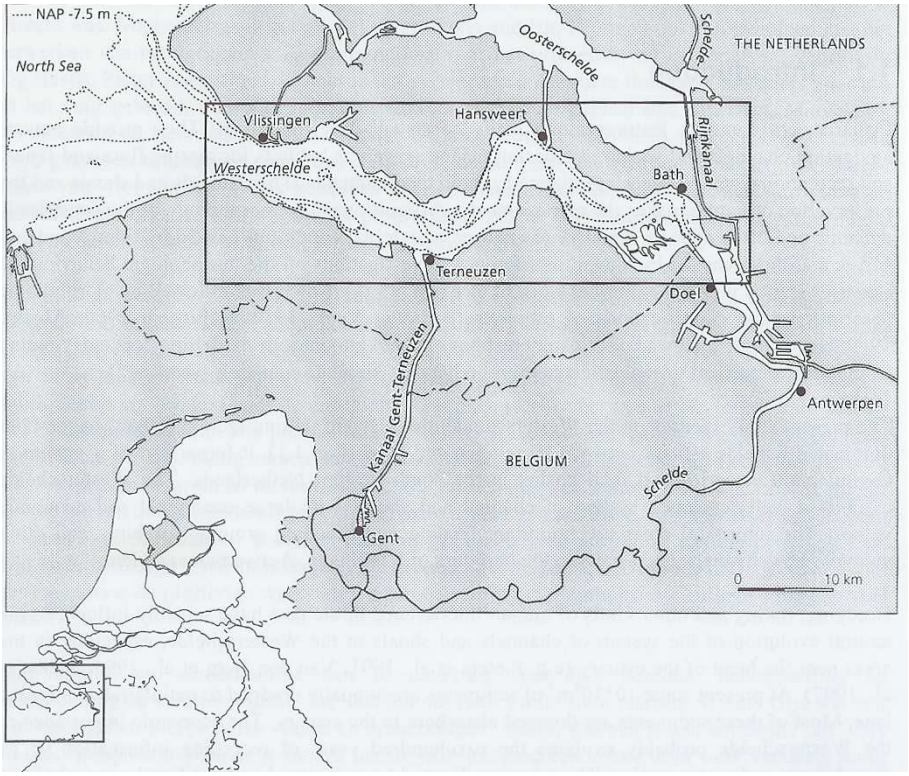

Figure 2.4: An overview of the Western Scheldt estuary. Source:[8].

2. *Connecting channels*, which exists of

   - bar channels, cutting through the shallow areas of the flood channel and linking two large main channels
   - cross channels, connecting the main ebb and flood channels
   - margin channels, linking large and small main channels along the estuarine boundaries

These channels display a repetitive channel pattern and are shown in Figure 2.5.

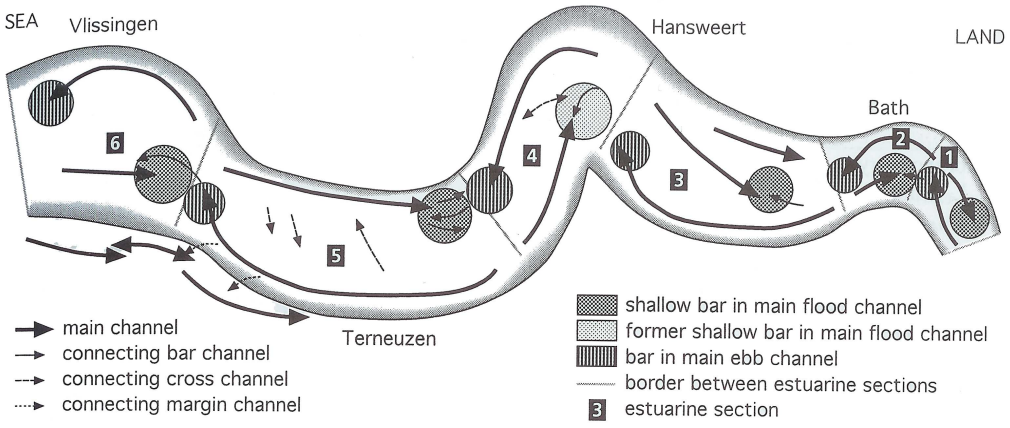

Figure 2.5: The channels in the Western Scheldt estuary. Source:[8].

Two different flows occur in the Western Scheldt. The *tidal flow* is the main driving force. Its volume at the mouth of the estuary is about 1 billion m^3. The mean range of the half-daily tide varies from about 3.8 m at Vlissingen (at the mouth) to about 5.2 m at Antwerp. Landward of Antwerp, the tidal range decreases to about 2m near Gent. Current velocities for an average tide range up to 1-2 m/s in the main channels [21]. The *river flow* on the other hand is less than one percent of the tidal volume with an outflow of only $2.5 \cdot 10^6$ m^3 per ebb or flood period [8].

2.2.2 Bed forms

The Western Scheldt bed is covered with specific bed forms. Wave-like forms occur in regular patterns and are usually called sand dunes or sand waves. If the velocity of the flow in the Scheldt estuary is sufficient to transport sediment either as bed load (particles moving along the bottom) or suspended load (particles moving in a stream without touching the bottom), an initially flat bed is deformed into a bed containing bed forms. Hence, the processes of erosion and deposition cause the formation of sand dunes. A characteristic bed form is shown in Figure 2.6. The sand dunes are not stationary, they usually migrate via bed load transport processes, with

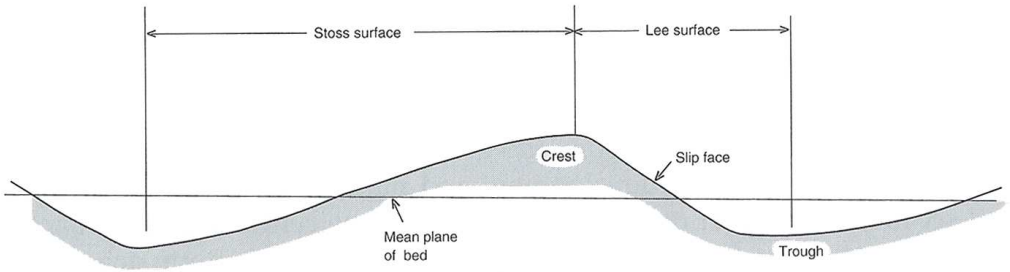

Figure 2.6: A typical subaqueous sand dune. Source:[20].

erosion occurring on the stoss surface and deposition being observed downstream form the crest, along the lee face [20]. The subaqueous bed forms can be characterized by wave length, amplitude, orientation, asymmetry and migration velocity.

A relative flat surface will develop into a series of relatively small-scale features called ripples, if the flow velocity is larger than a critical value. At somewhat higher velocities the ripples will transform into larger bed forms, named sand dunes. Dunes can either have a sharp or a flat crest. Sharp crested dunes present a degree of asymmetry similar to that of ripples, where dunes with a flat crest are more symmetrical in shape [20]. With a further increasing flow velocity at a certain stage no sand dunes or ripples can be found on the bed, the dunes are gradually transformed into a plane bed. Finally, under very high flow velocity conditions, bed features reappear and forms known as antidunes can occur. The four different stages are clearly shown in Figure 2.7. In the Scheldt estuary sand dunes (the second stage) of different sizes are present.

Generally, it is considered that subaqueous dunes scale with the flow depth, that is, the size increases with an increase in flow depth. Also the wave length and its amplitude may be correlated. Despite some variability in size and shape, sand dunes possess a striking degree of regularity or periodicity. The type of bed forms and its main characteristics depend to a large extent on the flow intensity. Furthermore, grain size plays a significant role in the development

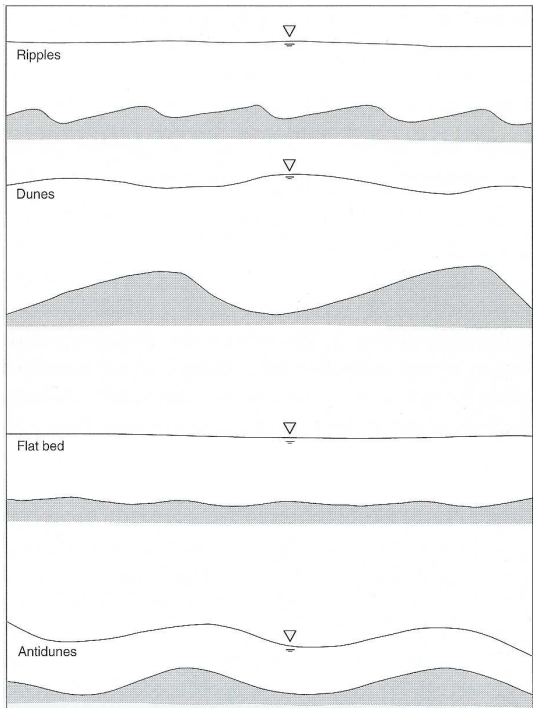

Figure 2.7: Four kinds of possible subaqueous bed forms. Source:[20].

of bed forms, and some bed form features will only be observed within a specific range of grain size [20].

2.2.3 Dredging

The Western Scheldt estuary connects one of the major harbours in the world, the port of Antwerp, with the North Sea. Of importance is to maintain access to the harbour on a scale that keeps up with current economic standards, implying a continuous increase in draught of the passing vessels. Guaranteeing access of large vessels means that the critical depth in the tidal channels has to be enforced by dredging. During the 1970's a first deepening campaign was executed. Also in the end of the 1990's, the Flemish government deepened and widened the navigation route to Antwerp [21].

In this dredging campaigns a strategy was chosen such that dredged material from the main channels was dumped into the side channels. In this way, dredging and dumping threatens the existence of the multiple channel system and can lead to a decrease in intertidal area and shallow water zones, which provide a habitat for various valuable species [21].

In the 'Long Term Vision', the governments of Flanders and the Netherlands considered the preservation of the multi-channel system as one of the main objectives. As a consequence, a new dump strategy was proposed and to investigate the effects a pilot project was executed. In this project dredged material is disposed near the shoal of Walsoorden.

2.3 The data sets

MBES data

As mentioned in Chapter 1, the sand dump near the shoal of Walsoorden was monitored at a two weeks interval. For this purpose the SIMRAD EM 3002 Dual head was used, being able to measure 508 depths per ping and this at 40 pings per second. Thus, 20.000 depths per second could be obtained. An area of approximately 11 km^2 had to be surveyed within one day, including a part of it located above low water level. A good mission design was therefore essential [12].

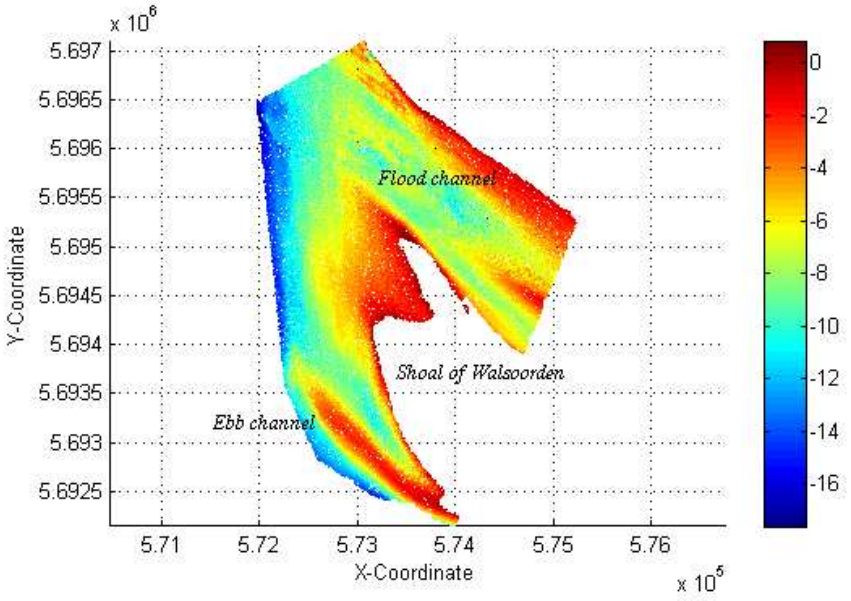

Figure 2.8: The points of the dataset at t_0 near the shoal of Walsoorden, with a rather shallow flood channel in the north east and an ebb channel in the deeper part just at the side of the study area.

In order to link the measurements of the multi-beam echo sounder to absolute coordinates, use was made of the LRK-GPS system. The base stations of this system cover the Western Scheldt completely. Afterward the coordinates were projected in the UTM system, zone 31. Furthermore, as attitude sensor a 'MRU-05' for the motion, combined with a 'Seapath 200' for the heading was used.

The surveys shown in Table 2.1 are used in this research for the analysis of the Western Scheldt near the shoal of Walsoorden. This dataset was interpolated on a rectangular 1 meter by 1 meter grid on forehand, resulting in data as for example shown in Figure 2.8. The disposal of the sand took place from the 17th of November until the 20th of December 2004. The dumping is also indicated in Table 2.1.

Survey	*Date*	*Action*	*day*
t_0	07-11-2004		7
t_1	23-11-2004	dump	23
t_2	29-11-2004	dump	29
t_3	13-12-2004	dump	43
t_4	22-12-2004	dump	52
t_5	10-01-2004		71
t_6	25-01-2005		86
t_7	03-02-2005		95
t_8	09-02-2005		101
t_9	17-02-2005		109
t_{10}	24-02-2005		116
t_{11}	04-03-2005		124
t_{12}	10-03-2005		130
t_{13}	17-03-2005		137
t_{14}	11-04-2005		162
t_{15}	02-05-2005		183
t_{16}	23-05-2005		204

Table 2.1: MBES-datasets used in this research.

Meteorological and tidal data

The exact date's of the measurements are known. Thus, it is possible to analyze the bathymetry in combination with the meteorological and tidal data.

A meteorological dataset, measured in Vlissingen, from the Royal Netherlands Meteorological Institute (KNMI) is used [9]. The most relevant attributes are:

- date
- prevailing wind direction
- daily mean wind speed
- maximum hourly mean wind speed
- daily mean temperature
- sunshine duration
- precipitation duration
- daily precipitation amount

In this study, rather extreme weather will be considered in relation to the estuary bed changes. The most important characteristics of such a weather are in this case the maximum hourly mean wind speed and the daily precipitation. Therefore, those attributes will be considered.

The ministry of transport, public works and water management provides information about the water level neat the shoal of Walsoorden [17]. Every ten minutes the mean water height in measured in centimeters with respect to the NAP. This tidal information will be analyzed in relation to the morphological parameter changes in the Scheldt estuary.

Chapter 3

Change detection

In this chapter the methods for detection of morphological changes in the Western Scheldt bed are described. This includes morphological parameter estimation of the subaqueous bed forms and deformation analysis of the global topography. Before theses methods can be applied, the coarse topography has to be separated from the sand dunes. This filtering procedure is described in Section 3.1. Section 3.2 deals with the two methods used for the determination of the parameter values, whereas Section 3.3 focuses on the deformation analysis.

3.1 Filtering

Processing the MBES data of the Scheldt estuary is strongly influenced by the presence of subaqueous dunes. Dunes and other periodic bed forms act as noise when assessing changes in global topography, e.g. for monitoring silting processes. Moreover, sand dune parameter estimation will be biased in case of local changes in topography, at for example steep terrain.

In order to solve these problems a signal decomposition step can be performed in which the global topography is separated from the bed forms [14]. In the Remote Sensing extensive use is made of spatial filters developed in the field of digital image processing. Spatial filtering is a 'local' operation as the pixel values in an original image are modified on the basis of the values of the neighbouring pixels only. The principles of these operations can also be used on our dataset.

Two well known spatial filters are the *low pass filter* and the *high pass filter*. Low pass filters are designed to emphasize low frequency features (large area changes) and deemphasize the high frequency components of an image (local detail), whereas the high pass filters do just the reverse [13].

The sand dunes cause a rather rough image, which means that the data changes abruptly over a relative small number of pixels. In order to subtract the topography from the original data, these local details need to be filtered out. To this end the low pass filter seems ideal, as it smooths the details in the original data and reduces deviations from the local average. Consequently, the residuals of the filtering process represent the subaqueous sand dunes.

Low pass filter

The low pass filter is a special application of the generic image processing operation called *convolution*. Convolving, and thus filtering an image involves the following procedures [13]:

1. The creation of a moving window, called a kernel, containing an array of weighting factors.

2. The kernel is moved throughout the original image, where the location at the center of the kernel in the output image is obtained by multiplying each coefficient in the kernel by the corresponding location in the original image and summarizing all the resulting products. This operation is performed for each pixel in the original image. An example is shown in Figure 3.1.

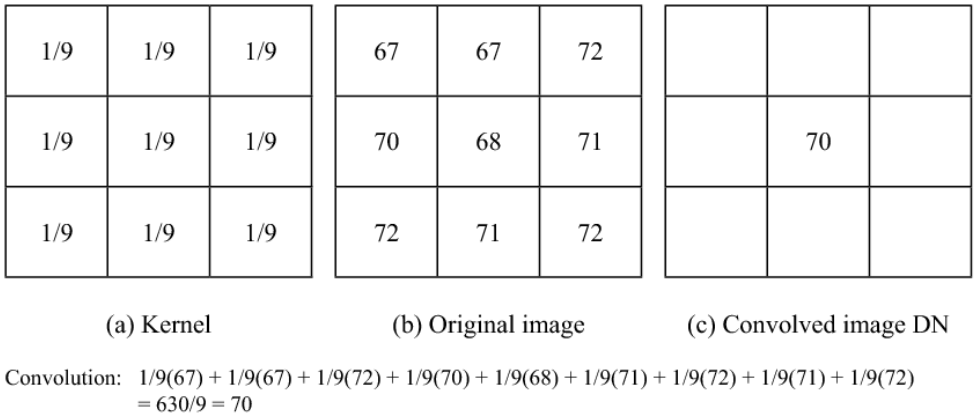

Figure 3.1: An example of a low pass filtering procedure of the original image (b) using a 3 × 3 pixel kernel with equal coefficients (a). The result is shown in (c). Source: [13].

With these procedures a low pass filtering operation can be performed. The influence of the filter depends directly upon the size of the kernel used and the values of the coefficients contained within the kernel. Thus, different filters are created by differing the kernel size or the kernel coefficients.

3.2 Parameter estimation

After the separation of the subaqueous dunes and the large scale topography, the parameters of the bed forms can be estimated. Three morphological parameters describing these bed forms are considered:

1. *The orientation* of a dune field is the direction clock wise from the North in which the maximal variation in depth occurs.

2. *The amplitude* of a sand dune is defined as half the vertical distance between its highest and lowest point.

3. *The wave length* is the horizontal distance, in the direction of the dune field orientation, between two consecutive dune peaks (maxima) and troughs (minima).

The parameter values can be estimated using two different approaches, i.e. *the profile line based method* and *the variogram based method*.

3.2.1 The profile line based method

In the first technique for the determination of the parameter values use is made of profiles. Points from the sand dunes data set which define a linear line with a certain orientation will be analyzed in this method. The basis of this method lies in the identification of local extrema in profiles. These can be discovered by looking for each point at a n number of its neighbours and determine whether or not the center point has the maximal or minimal value. Drawing profile lines is a rather simple method in order to estimate the orientation, amplitude and wave length of the bed forms.

The *orientation* can be obtained by making use of the fact that along a profile the wave direction is indicated by the orientation of the minimized distance between two waves. The way to estimate its value is to draw profiles through a grid point at regular angle intervals. The angle of the profile with the highest number of local extrema gives the dune orientation.

The *amplitude* can be determined from the vertical distance between the peaks and troughs. As the global topography is filtered out, the amplitude A can be estimated after calculating the difference between the mean maxima and minima, reading:

$$A = \frac{1}{2}\left(\frac{\sum d_{max}}{N_p} - \frac{\sum d_{min}}{N_t}\right) \tag{3.1}$$

with d_{max} the depth of a peak point, d_{min} the depth of a trough point, N_p and N_t the numbers of peaks and troughs.

The *wave length* is estimated by simply dividing the range of the wave orientation profile by half the number of the local extrema (a single sand dune consists of two extrema: one peak and one trough). Hence the wave length λ can be calculated as:

$$\lambda = \frac{r}{\frac{1}{2}(N_p + N_t)} \tag{3.2}$$

with r the range, N_p and N_t the numbers of peaks and troughs.

Obviously, the amplitude and wave length can differ along a certain profile. In this case only one estimate of a parameter in a certain, rather small area is wanted. The profile line based method can be performed for a large amount of different profiles. Consequently, the mean and standard deviation σ of the amplitude and wave length can be calculated. The standard deviation is defined as:

$$\sigma = \sqrt{\frac{1}{n-1}\sum_{i=1}^{n}(z_i - m)^2} \tag{3.3}$$

with n the number of parameter values, z_i the i-th parameter value and m the mean of the parameter values.

In the profile based method it is possible to obtain grid-point wise an orientation, amplitude and wave length result. However, as the orientation of a small area is assumed to be similar for all the points, the orientation will not always be estimated for each point, but chosen for the whole region. To underline this difference, the method estimating a grid point wise orientation will be called *the classification method*, whereas the method using one orientation for the whole area will be named *the profile line method*.

3.2.2 The variogram based method

The second approach for the estimation of the parameter values makes use of a variability analysis. To this end, a well known tool in the field of applied geostatistics is used: the variogram.

The variogram

The variogram γ is a measure for the average variability between the data points at a distance h [4]. Let p_i and p_j denote the horizontal position and z_i and z_j the depth of the observations i and j. The raw variogram or variogram cloud, is a scatter plot between half the square of the difference between the observed values, $\frac{1}{2}(z_i - z_j)^2$ and the separation distance, $\|h\| = \|p_i - p_j\|$. For n measurements this leads to $n(n-1)/2$ pairs. To obtain the experimental variogram, the axis of separation distance is divided into consecutive intervals and the average of each interval is computed. Hence, the experimental variogram can be calculated as:

$$\gamma([h_k]) = \frac{1}{2N_k} \sum_{(z_i, z_j) \in [h_k]} (z_i - z_j)^2 \tag{3.4}$$

with $[h_k]$ the k-th distance class with respect to the horizontal distance between p_i and p_j and N_k the number of data pairs within this k-th distance class

Through the experimental variogram a continuous mathematical function can be fitted, called a theoretical variogram. The advantage is that one can deduce a variability value for any possible distance. The total procedure is demonstrated in Figure 3.2. It shows the steps for the computation of an experimental and theoretical variogram:

- Create a variogram cloud
- Divide into consecutive intervals
- Calculate the group average, obtaining an experimental variogram
- Estimate a continuous function through the points, resulting in a theoretical variogram

Usually the average variability between the values increases with an increasing distance, until it reaches at a certain *range* the maximal variability, called the *sill*. If there is a measurement error or spatial variation at a distance smaller than the shortest sampling interval, a *nugget* effect can appear. This is a discontinuity at the origin of the variogram. These three parameters, the sill, range and nugget, are often used to characterize the variogram.

The variogram as presented above is independent of its orientation. It is assumed that the variability does not differ with the direction but only with the distance. This is however not always the case, for example our sand dunes do not have the same variability perpendicular or parallel to the crest. This phenomenon is called anisotropy and if it occurs, it is useful to calculate a directional variogram only including pairs with a certain orientation.

Parameter estimation

Some variograms show decreasing segments or cyclicity. In such a model first the variability is increasing to a maximum value after which it drops to a local minimum. These are indicated as 'hole-effect' structures and can have a physical interpretation. Most often the hole effects

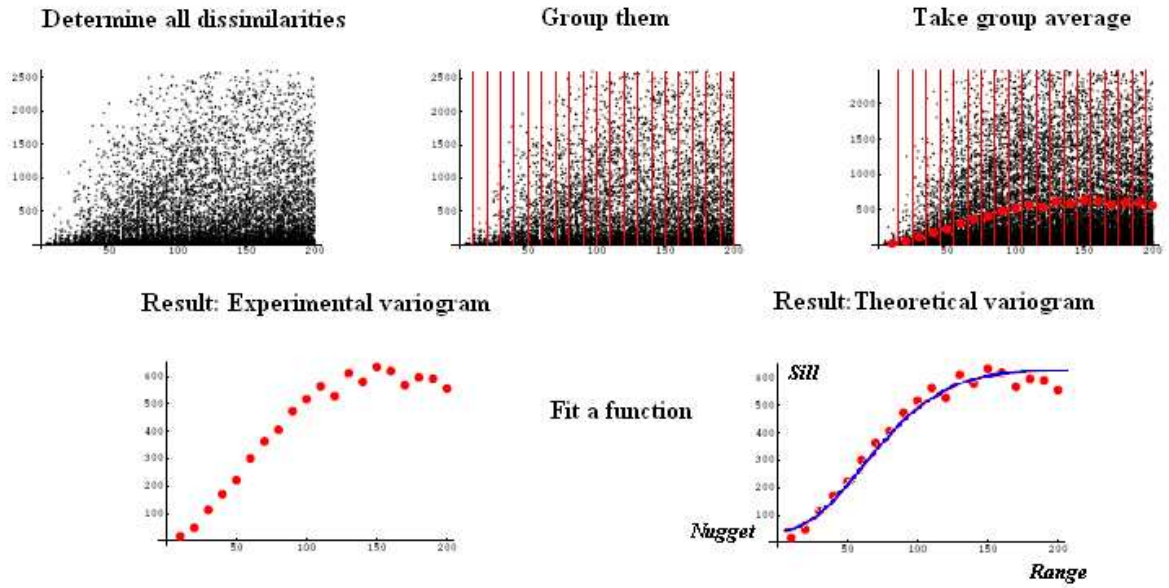

Figure 3.2: The steps for the computation of variograms. Source: [Lecture notes *Multivariate data analysis*].

indicate a form of periodicity [19]. In the case of the bed forms in the Western Scheldt the directional variograms do have a cyclical form, which is due to the presence of sand dunes. Subsequently, the form of the variograms gives information about the presence of the sand dunes, but it turns out it also gives the opportunity to estimate its parameters.

The sand dune *orientation* can be detected by taking the anisotropy into account. The changes in variability at different directions give indications about the orientation. Along the dune crests, the average variability will be minimal and the hole effect in the variogram will disappear. The angle perpendicular to this directional variogram gives the dune orientation.

The *amplitude* is directly linked to the maximum value of the variogram before the hole effect occurs. The directional variogram, computed in the dune orientation, indicates the variability of the data as a function of its distance. It is calculated with the square of the difference between values at a certain distance. As the experimental variogram is computed by the average of the scatter values, this square root of this value is approximately half the maximum variability between two points separated by half the wave length. The amplitude is defined as half the range between peaks and troughs. Hence, it can be obtained by calculating the square root of the maximum value of the directional variogram $\gamma(h)$:

$$A = \sqrt{\max \gamma(h)} \tag{3.5}$$

Finally, also the *wave length* of the subaqueous dunes can be estimated from the directional variogram. A drop (a hole effect) in the experimental variogram indicates a correlation between the $z-$values at the points in the specific distance class. An estuary bed covered with sand dunes will also have this hole effect; the values at a entire wave length separated from each other will have a smaller variability than the values separated at half the wave length. Consequently,

if a directional variogram is made in the direction of the sand dunes, the distance of the first hole effect indicates the wave length of these bed forms.

The variogram cloud will be calculated for a subset of the data points, as taking all the points into account will cause enormous calculation time problems. This gives us also a way to estimate the variance of the wave length and amplitude. It can be calculated following the bootstrapping method. The principle idea behind bootstrap is simple. Suppose we draw a sample $\mathbf{s} = (s_1, \ldots, s_n)$ from some unknown probability distribution $F(s)$. Insight in a complicated estimator $K(\mathbf{s})$ of a parameter $k(F)$ of $F(s)$ can be gained by studying the properties of the corresponding estimator $K(\mathbf{s}^*)$ on the space of samples $\mathbf{s}^* = (s_1^*, \ldots, s_n^*)$ drawn from a data-based approximation $F_n^*(s)$ to $F(s)$. This method assumes that not only $K(\mathbf{s})$ and $K(\mathbf{s}^*)$ have similar distributions, but also $K(\mathbf{s}) - k(F)$ and $K(\mathbf{s}^*) - k(F_n^*)$ [11]. The variance of the estimator $K(\mathbf{s})$ can be estimated by the variance of the corresponding estimator $K(\mathbf{s}^*)$ on the bootstrap sample space. Because the variance or standard deviation of $K(\mathbf{s}^*)$ is difficult to calculate exactly, independent bootstrap samples $\mathbf{s}_b^* = (s_{b1}^*, \ldots, s_{bn}^*)$ for $b = 1, \ldots, B$ are used. The standard deviation of $K(\mathbf{s}^*)$ can now be approximated by [11]:

$$\sigma_{K^*} = \frac{1}{B-1} \sum_{b=1}^{B} (K(\mathbf{s}_b^*) - \hat{E}(K)^*)^2 \tag{3.6}$$

where

$$\hat{E}(K)^* = \frac{1}{B} \sum_{b=1}^{B} K(\mathbf{s}_b^*) \tag{3.7}$$

In our practical situation this means that a lot of variogram clouds are made using a different sample dataset. Subsequently, the best continuous variogram is fitted through the data and the estimations for the parameter values are calculated. Now, by computing for B different randomly chosen subsets the variogram, the mean and the variance of the morphological parameter values can be obtained.

3.3 Deformation analysis

Measurements always contain some noise and uncertainties. That is the reason why redundant measurements are performed; with these extra information one can check for errors and also increase the accuracy. The problem, however, with redundant measurements is the almost unavoidable appearance of inconsistent systems of equations. The theory that faces the problem of these inconsistent systems, the adjustment theory, is explained in Section 3.1. It solves the system in an optimal way and estimates the unknown parameters. On the other hand, the testing theory described in Section 3.2, deals with the detection of errors in the measurements and in the mathematical model. Together they form the mathematical basis for the theory of deformation analysis (Section 3.3).

3.3.1 Adjustment theory

The relation between the $m \times 1$ observation vector $\underline{y}$ and the unknown $n \times 1$ parameter vector x is usually expressed with the help of a model matrix A. This matrix describes the model of observation equations and reads [22]:

$$\underline{y} = Ax + \underline{e} \tag{3.8}$$

Observations are stochastic instead of deterministic. This influence is modeled in the measurement errors $\underline{e}$. The adjustment theory estimates the unknown parameters x of the observation equations in the best possible way, using the principles of least-squares.

If one assumes that the expectation of the observation errors equals zero, Eq. 3.8 can also be written as:

$$E\{\underline{y}\} = Ax; \quad D\{\underline{y}\} = Q_y \tag{3.9}$$

with $E\{.\}$ the expectation, $D\{.\}$ the dispersion and Q_y the variance-covariance matrix of the observations.

A solution for this model can be achieved using the principle of Best Linear Unbiased Estimation (BLUE). Figure 3.3 illustrates this principle, in which the variance of the estimator is minimized. The mathematical solution of the best estimator $\underline{\hat{x}}$ reads:

$$\underline{\hat{x}} = (A^T Q_y^{-1} A)^{-1} A^T Q_y^{-1} \underline{y} \tag{3.10}$$

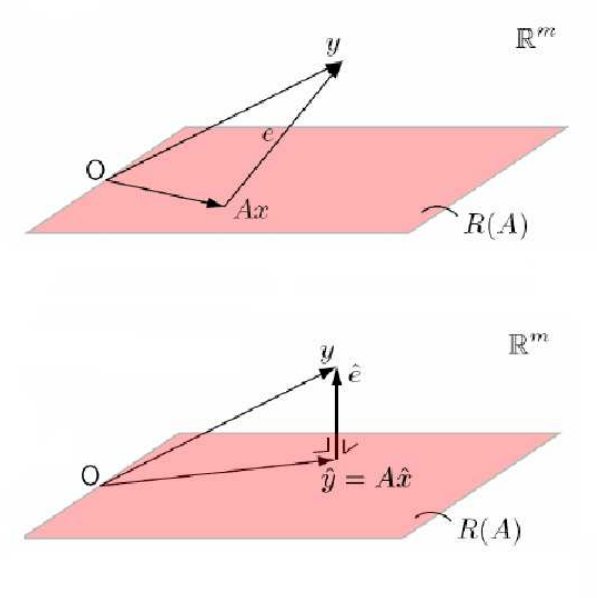

Figure 3.3: Upper plot: an (not the best) estimation of the parameters x and e. Lower plot: The best estimation of the unknown parameters x and e, using the least square principle.

Using this solution the estimations of the observations $\underline{\hat{y}}$ and errors $\underline{\hat{e}}$ can easily be obtained:

$$\underline{\hat{y}} = A\underline{\hat{x}} \tag{3.11}$$

and

$$\underline{\hat{e}} = \underline{y} - \underline{\hat{y}} \tag{3.12}$$

Applying the propagation law of variances and covariances leads to:

$$Q_{\hat{x}} = (A^T Q_y^{-1} A)^{-1} \tag{3.13}$$

$$Q_{\hat{y}} = AQ_{\hat{x}}A^T \tag{3.14}$$

$$Q_{\hat{e}} = Q_y - Q_{\hat{y}} \tag{3.15}$$

with $Q_{\hat{x}}$, $Q_{\hat{y}}$ and $Q_{\hat{e}}$ the variance covariance matrices of the best estimators of respectively $\underline{\hat{x}}$, $\underline{\hat{y}}$ and $\underline{\hat{e}}$.

3.3.2 Testing theory

Now that the problem of redundant measurements is solved, the question is whether or not the mathematical model is correct. If that is not the case the BLUE method does not lead to optimal results. Hence, the chosen model has to be tested and if necessary corrected.

The testing theory is based on the formulation of hypotheses. In principle the least-squares residuals are compared with what can be expected if the model is valid [18]. The model used in the adjustment procedure is here called the null hypothesis H_0. If this model is not correct an adaption is needed, which will be formulated in the alternative hypothesis H_A [23]:

$$H_0 : E\{\underline{y}\} = Ax; \quad D\{\underline{y}\} = Q_y \tag{3.16}$$

$$H_A : E\{\underline{y}\} = Ax + C\nabla; \quad D\{\underline{y}\} = Q_y \tag{3.17}$$

Thus, the null hypothesis states that the mathematical model is correct, while in the alternative hypothesis the model needs an extension ∇ specified by the matrix C. In order to be able to test these models, a test statistic $\underline{T}$ can be calculated:

$$\underline{T}_q = \underline{\hat{e}}_0^T Q_y^{-1} \underline{\hat{e}}_0 - \underline{\hat{e}}_A^T Q_y^{-1} \underline{\hat{e}}_A \tag{3.18}$$

with q the number of degrees of freedom, $\underline{\hat{e}}_0$ and $\underline{\hat{e}}_A$ the least square residual vector under respectively the null hypothesis and the alternative hypothesis. It is also possible to express the test statistic without the term $\underline{\hat{e}}_A$:

$$\underline{T}_q = \underline{\hat{e}}^T Q_y^{-1} C_y (C_y^T Q_y^{-1} Q_{\hat{e}} Q_y^{-1} C_y)^{-1} C_y^T Q_y^{-1} \underline{\hat{e}} \tag{3.19}$$

The probability density function of a test statistic is a central chi-squared distribution with q degrees of freedom $\chi^2(q, 0)$ under the null hypothesis. The expectation of the test statistic is equal to q, $E\{\underline{T}_q\} = q$. Under the alternative hypothesis, the test statistic has a non-central chi-squared distribution $\chi^2(q, \lambda)$ and the expectation of the test statistic reads $E\{\underline{T}_q\} = q + \lambda$, where λ is the non-centrality parameter which can be expressed as:

$$\lambda = \nabla^T C_y^T Q_y^{-1} Q_{\hat{e}_0} Q_y^{-1} C_y \nabla \tag{3.20}$$

Subsequently, the degrees of freedom q can be defined as the rank of C_y. Its range is given by $1 \leq q \leq m - n$. If the null hypothesis is not correct, the test statistic will tend to become larger than if the hypothesis is correct. The area α in the probability density function in which the test statistic can occur while it is true, is called the level of significance. Hence, α is the chance that H_0 is rejected when in fact H_0 is true.

The testing procedure is a comparison between the calculated test statistic, based on the least-squares residuals of the adjustment, and a certain value. This value, the critical value k_α, is computed based on the level of significance α. If the model is correct, one expects smaller least-squares residuals than in the case the model is false. This is clearly visible in the χ^2-distribution, as can be seen in Figure 3.4.

By testing the hypotheses one can make two mistakes [23]:

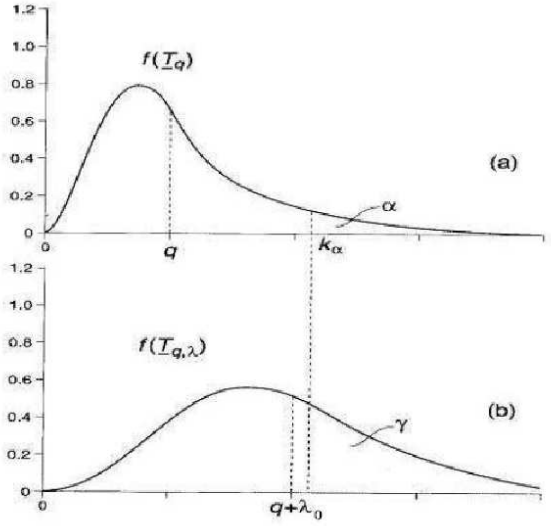

Figure 3.4: The χ^2-distribution of the test statistic $\underline{T}_q$ when H_0 is true (a) or H_A is true (b). Source: [18].

- Type 1 error: Rejection of H_0 when in fact H_0 is true.
- Type 2 error: Acceptance of H_0 when in fact H_0 is false.

The first error, the false alarm is indicated by α. Its value describes the probability that a sample falls in the critical region when the model is true. By choosing this α one accepts a certain percentage of unjust rejections. The second error, representing a missed alarm is denoted by β. Then, the power of the test γ can be indicated as $1 - \beta$. Of course one wants to have these errors as small as possible, but as one decreases α, β tends to become larger. To overcome this problem we follow the Neyman-Pearson principle, which states that the level of significance α should be chosen and then minimize the size of β [23]. With a known α one can calculate the critical value k_α and formulate the generalized likelihood ratio test as:

$$\text{reject } H_0 \text{ if } \underline{T}_q > k_\alpha \text{ or if } \underline{T}_q / k_\alpha > 1. \tag{3.21}$$

3.3.3 Deformation detection

The theory of deformation analysis is completely based on the adjustment- and testing theory as described before. The approach however, is totally different. In the traditional situation, like leveling applications, one knows the mathematical model and checks whether or not the observations agree with it. In the deformation analysis, on the contrary, the model is unknown and estimated using the observations.

The purpose is to model the changes in the object. The first step is to perform a stability analysis. Here, one checks if there are any changes at all. Assuming the same reference frame for all the observations, the null hypothesis H_0 for stability in the 1-dimensional case reads:

$$H_0 : E\{ \begin{bmatrix} \underline{d}_{p_1} \\ \vdots \\ \underline{d}_{p_m} \end{bmatrix} \} = \begin{bmatrix} 1 \\ \vdots \\ 1 \end{bmatrix} d_p \tag{3.22}$$

where $\underline{d}_{p_i}$ indicates the measured depths at position p at sounding moment i. One wants to test this without specifying another hypothesis, because it is not known if there are one or more errors in the model and totally unclear what kind of misspecifications are expected under H_0. First a check on the overall validity of H_0 is performed. The null hypothesis is tested against the most relaxed alternative hypothesis, which reads:

$$H_A : E\{ \begin{bmatrix} \underline{d}_{p_1} \\ \vdots \\ \underline{d}_{p_m} \end{bmatrix} \} \in \mathbb{R}^m \tag{3.23}$$

No restrictions are placed on $E\{\underline{d}_{p_i}\}$, the observations are completely free. By choosing $q = m - n$, the number of explanatory variables that are added on H_0 in order to form H_A are such that the redundancy of the linear model under H_A equals zero. This means that $\hat{\underline{d}}_A \equiv \underline{d}$ and $\hat{\underline{e}}_A \equiv 0$. Using Eq. 3.18 the test statistic becomes [23]:

$$\underline{T}_q = \hat{\underline{e}}^T Q_y^{-1} \hat{\underline{e}}. \tag{3.24}$$

This test is called the overall model test and gives an indication whether or not the model is correct.

If the test fails, the model is not an overall valid model. Therefore another mathematical model has to be chosen. It is possible to extend the model with $C\nabla$, but one can also formulate a complete different model, e.g. a sine or cosine model. Until a mathematical overall model is accepted, the null hypothesis is tested against the most relaxed hypothesis, formulated in Eq. 3.23.

Having found a null hypothesis accepted by the overall model test, one can extend it further with $C\nabla$. As now an idea about a specific alternative hypothesis is known (the extension of the accepted null hypothesis in the overall model test), one can test with Eq. 3.18 or Eq. 3.19 H_0 against H_A and determine whether or not this extension is significant. The number of degrees of freedom q equals the rank of the design matrix of the model extensions. A polynomial model can be used for this extension [24]:

$$p_n(d) = \sum_{j=0}^{n_t} a_j t^j \tag{3.25}$$

with n_t the time degree, in this case equal to the degree of the polynomial. It can be written as the following observation equation:

$$E\{\underline{d}_i\} = a_0 + a_1 t^1 + a_2 t^2 + \cdots + a_{n_t} t^{n_t} \tag{3.26}$$

Hence, in the case the hypothesis of Eq. 3.22 is accepted in the overall model test one can think of formulating an alternative hypotheses by increasing the degree of the polynomial and thus extending the model, leading to:

$$H_A : E\{ \begin{bmatrix} \underline{d}_{p_1} \\ \vdots \\ \underline{d}_{p_m} \end{bmatrix} \} = d_p + C\nabla \tag{3.27}$$

with for example an extension

$$C = \begin{bmatrix} t_1 \\ \vdots \\ t_m \end{bmatrix} \quad \text{and } \nabla = a_1 \tag{3.28}$$

or

$$C = \begin{bmatrix} t_1 & t_1^2 \\ \vdots & \vdots \\ t_m & t_m^2 \end{bmatrix} \quad \text{and } \nabla = \begin{bmatrix} a_1 \\ a_2 \end{bmatrix} \tag{3.29}$$

The calculated test statistic has a χ^2 distribution with in the first extension a number of degrees of freedom $q = 1$ and in the second extension $q = 2$. If one of these extended hypotheses is accepted by the test statistic as formulated in Eq. 3.18 or Eq. 3.19 it will function as the new null hypothesis. Subsequently, new extensions of the hypotheses can be formulated and tested on significance.

Estuary floor models

For the modeling the global changes in the estuary bed, point wise models are formulated, including:

- Local stability
- Local constant velocity
- Local constant acceleration

These hypotheses can be found in the low order degrees of the polynomial model Eq. 3.26, with for stability:

$$E\{\underline{d}_i\} = a_0 \tag{3.30}$$

with a_0 the constant depth.
The model for constant velocity:

$$E\{\underline{d}_i\} = a_0 + a_1 t^1 \tag{3.31}$$

The simple mechanical equation of uniform motion reads $d(t) = d(0) + v \cdot t$. One can easily see that in this hypotheses the velocity v of the uniform motion is represented by a_1.
Finally, the model for constant acceleration reads:

$$E\{\underline{d}_i\} = a_0 + a_1 t^1 + a_2 t^2 \tag{3.32}$$

The well known model of uniform acceleration reads $d(t) = d(0) + v(0) \cdot t + \frac{1}{2} a \cdot t^2$. Hence, also these coefficients of the polynomial model have a physical meaning with a_1 means the constant velocity v and a_2 represents half the constant acceleration a.

Quality

The acceptance of a hypothesis depends on the residuals $\hat{e}$ between the data and the proposed model, the variance-covariance matrix Q_y and the critical value k_α. This critical value depends on the level of significance α and the degrees of freedom $m - n$. The α, the probability that H_0 is rejected when in fact H_0 is true, can be chosen. The degrees of freedom on the other hand are fixed, depending on the particular alternative hypothesis against which one wants to test H_0. Consequently, the choice of the Q_y-matrix is rather important for the outcome of the deformation analysis.The Q_y-matrix models the stochastic influences. The variance and covariances can be calculated or assumed.

By the calculation use can be made of the propagation law of variances. Let $\underline{U}$ be a vector

of stochastic variables, calculated with a model matrix A from the vector of stochastic variables $\underline{V}$. The propagation law reads:

$$\underline{U} = A\underline{V} \Rightarrow Q_U = A^T Q_V A \tag{3.33}$$

with Q_U and Q_V the variance covariance matrices of respectively $\underline{U}$ and $\underline{V}$.

If there is no correlation assumed, and thus the Q_V-matrix consists of numbers on the diagonal and zeros elsewhere, the propagation law from Eq. 3.33 simplifies into:

$$\underline{u} = a\underline{v} \Rightarrow \sigma_u^2 = a^2\sigma_v^2 \tag{3.34}$$

The variance-covariance matrix can also be assumed. However, for a good choice of the standard deviation σ, one must have insight in its meaning in relation to hypotheses testing. The σ is used to determine whether or not the residuals between the observations and the proposed model can be explained by the variance. If this σ is large, the restrictions for the models are less strict. Therefore the standard deviation is just a scaling factor for the χ^2 distribution of the test statistic. Now, if a large σ is used, more points will be assumed to follow the hypothesis.

Subsequently, if one tests two hypotheses against each other, the residuals $\hat{e}$ becomes significantly smaller when the model fits better. One tests the need for extending the null hypothesis, by calculating the test statistic $\underline{T}_q$ with the same Q_y-matrix and thus the same variance. The σ is now not that important, because the same scaling factor for the χ^2 distribution is used in both hypotheses, and therefore a significant extension can be detected.

Chapter 4

Classification

The Western Scheldt bed is covered with bed features having a wave-like form. These patterns are not uniform for the whole estuary; the wave length, amplitude and direction differ, but are the same in a certain, smaller area. By taking a closer look at the bed forms, more insight in the dynamic structures of the Western Scheldt can be gained from the parameters of these sand waves. Moreover, as the morphology of the multi-channel estuary strongly varies with location, a spatially grouping procedure may be necessary for a good deformation analysis and parameter estimation result. The detection of the changes in the estuary bed is less complex if the bed forms are uniform. These are the main reasons for the classification of the complete data set at one survey.

Because of the larges differences in bed form parameters in our area, a first step is to determine the amplitude and wave length for each point in one epoch, t_0. In Section 4.1 the estimation of the parameters is described using the *classification method*, explained in Section 3.2. The objective in Section 4.2 is to perform a generalization procedure on the data set. Each single point will be categorized into different classes of amplitude and wave length.

4.1 Morphological parameters

Before the points can be classified, the morphological parameters of that point have to be estimated. One wants to know how large its amplitude and wave length is. The difficulty however is, that one single point does not determine the wave length nor the amplitude. In order to calculate the parameter values the location has to be analyzed together with its neighbours.

4.1.1 Wave direction

Before one can determine the amplitude and wave length of the bed forms, the local direction of the sand waves has to be estimated. This is possible by making use of the fact that in the wave direction the distance between two waves is minimized. The procedure used in this research is as follows:

- Set a certain angle w.r.t the azimuth and create a profile line
- Increase this angle with a small step and create a new profile line
- Perform this operation until the circle is completed
- Calculate the number of local extremes for each profile

Now, all the information needed for estimating the wave direction is obtained. One can easily understand that the profile line with the maximum number of local extremes, i.e. with the most peaks and troughs, relative to the length, has to be the line in the wave direction. Therefore, the orientation of the sand waves can be determined.

Here, an increment angle of 11.45 degree (0.2 rad) is used, leading to a star-like form with the point of interest in the center, as can be seen in Figure 4.1. Of course, the data has to be corrected for topography before the number of local extremes gives meaningful information. Therefore, the total data is filtered, i.e. the parameter estimation is based on the residuals between the dataset and the filtering operation.

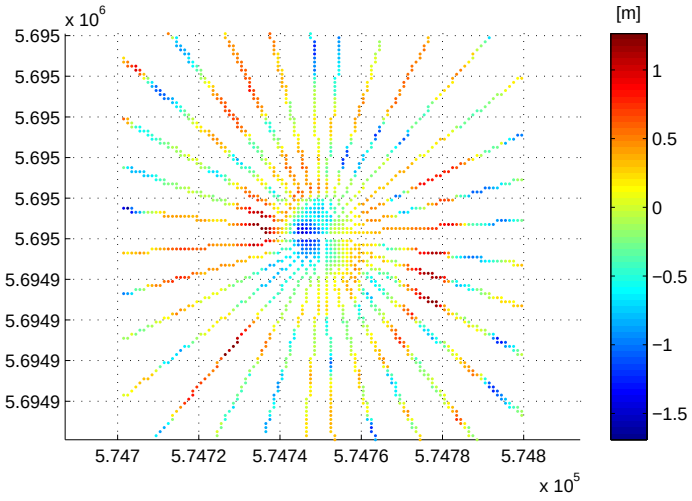

Figure 4.1: The star helping to determine the wave direction.

Figure 4.2 shows an overview of the estimated wave direction. This direction looks rather uniform, with a dominating wave length of 2.1 rad. This sand dune orientation can be explained by the presence of the dominating main flood channel in this orientation, as is shown in Figure 2.5. The deviating wave directions in the south and eastern part of the study area agree with this explanation as in these regions different main channels occur. Because of the clear dominance for almost the whole area the wave direction will not be generalized further.

4.1.2 Wave length and amplitude

Having obtained information about the direction of the sand waves, the estimation of the wave length and amplitude parameters is rather easy. These parameters follow directly from the local extremes. The wave length can be estimated by simply dividing the length of the wave direction profile by half the number of local extremes, because one single sand wave consists of two extremes: one peak and one trough. The amplitude can be obtained by calculating the mean difference between the peaks and the troughs. This leads to the results shown in Figure 4.3. The amplitude differs in the range between 0.2 m and 0.7 m. On the other hand, the wave length reaches values between 11 m and 27. The results demonstrate, as one expects, a clear spatial correlation in the wave length and amplitude parameters. Furthermore, there seems to be a

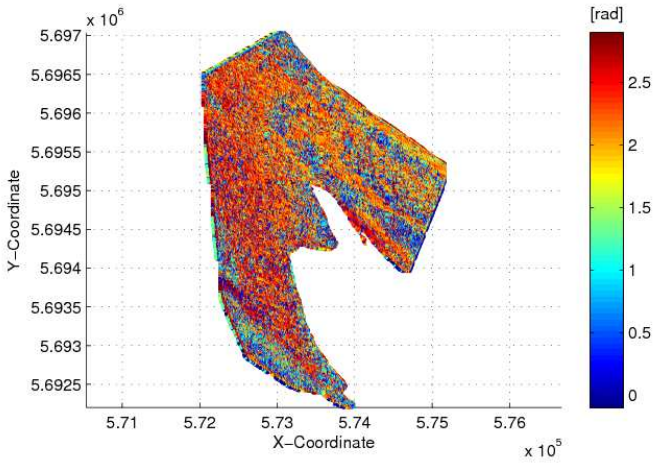

Figure 4.2: The wave direction parameter.

remarkable correspondence between the spatial correlated areas in the wave length plot and the amplitude plot.

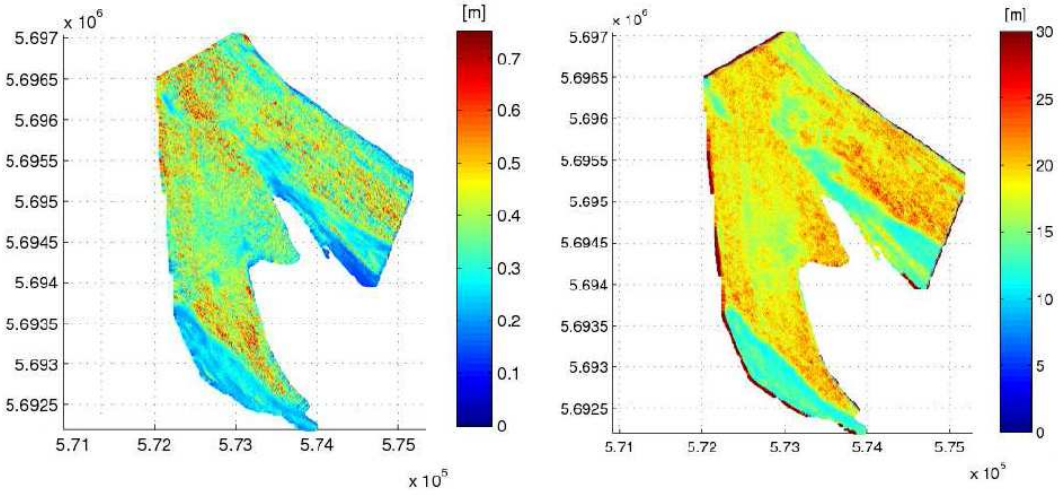

Figure 4.3: The amplitude (left) and the wave length (right) parameter.

4.1.3 Remarks

Using this classification method, disturbances in the estimated parameters can occur caused by three possible reasons:

1. In order to get good results, the topography is first filtered out, using a kernel of 25×25 meters. The size of this kernel can influence the amplitude more than the wave length. If the kernel is too small, the global topography will contain partly the sand wave. This does not have large implications for the wave length, because subtracting two waves with the same wave length leads to a wave with identical wave length, however the calculated amplitude is in that case smaller than in reality.

2. A possible error is the determination of one extra local extreme by estimating the wave length. If one takes the relative short profile line of 100 meters into account, the acceptance of one extra peak or trough at the end of the profile will have a significant influence and can cause unexpected differences between neighbouring points.

3. By using profile lines, the edge points can give bad results. The problem is that in this method the estimation of the parameters depends on its neighbours. The points on the edge of the data set do not have enough points for making sufficient large profile lines. Therefore, as one can see in the western part of Figure 4.3, the results in the wave length parameters can be disturbed.

4.2 Generalization

Now, for each point the length and amplitude of the sand waves at t_0 has been estimated. In order to get a better overview and correct for the erroneous results, the point-wise results are generalized and categorized. Therefore, threshold values will be introduced and morphological operations will be used to generalize the spatial correlated parameters.

4.2.1 Segmentation

Looking at Figure 4.3, it seems reasonable to divide the wave length and amplitude in four different classes. The threshold values used to segmentate the parameters are for the amplitude $Tr_a = (0.3, 0.4, 0.5)$ and for the wave length $Tr_w = (15, 18, 21)$. The result of this categorization is shown in Figure 4.4.

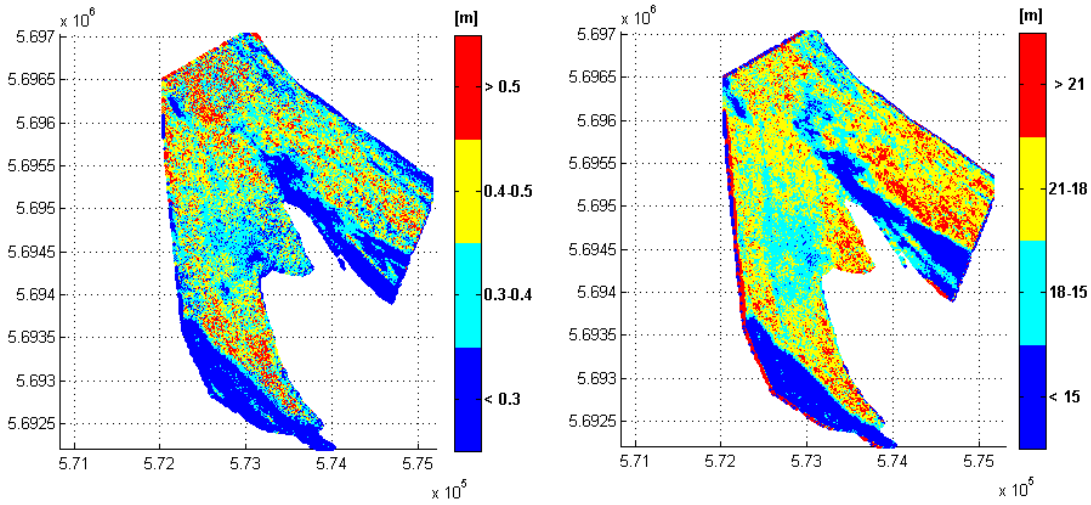

Figure 4.4: The amplitude (left) and wave length (right) parameters after the categorization.

After dedicating each value to a certain class, we obtain a four-color plot for the wave parameters. In reality, we know that the points are strongly spatially correlated. Certain values of one point are also expected to be found by the neighbours, because one point does not describe a sand wave; it must be seen in combination with the neighbouring points. One also wants this spatial correlation in the generalized result. Morphological operations can help to reach this objective.

4.2.2 Morphological operations

Morphology is the study of topology or structure of objects. Morphological operations then, refer to processes which changes the objects form. Most operations can be defined in terms of two basic operations: *dilation* and *erosion* [7]. Also the *closing* and *majority* operation will be discussed.

Erosion

Erosion is a shrinking operation which needs two different inputs: The image to be eroded and a set of points known as structuring element or kernel. If the origin of the structuring element is laid over a pixel in the image, the result for the erosion operation is the minimum value of all the points in the image selected by the structuring element. The example of Figure 4.5 makes this operation clear. Erosion is more formally described as follows [7]:

Suppose the object $\mathbf{X}$ and the structuring element $\mathbf{B}$ are represented as sets in two-dimensional Euclidean space. Let $\mathbf{B}_x$ denote the translation of $\mathbf{B}$ so that its origin is located in x. Then the erosion of $\mathbf{X}$ by $\mathbf{B}$ is defined as the set of all points x such that $\mathbf{B}_x$ is included in $\mathbf{X}$, that is:

$$\mathbf{X} \ominus \mathbf{B} = \{x : \mathbf{B}_x \subset \mathbf{X}\} \tag{4.1}$$

Dilation

In Figure 4.5 a clear example of a dilation operation can be seen. In contrast with the erosion operation, the result of the dilation operation is the maximum value of all the point in the image selected by the structuring element. It enlarges the input image, reading formally [7]:

The dilation of $\mathbf{X}$ by $\mathbf{B}$ is defined as the set of all points x such that $\mathbf{B}_x$ hits $\mathbf{X}$, that is, they have a nonempty intersection:

$$\mathbf{X} \oplus \mathbf{B} = \{x : \mathbf{B}_x \cap \mathbf{X} \neq \phi\} \tag{4.2}$$

Closing and Majority

As erosion and dilation are the two basic morphological operations, others can be derived of it. A useful operation is the morphological closing. This blocks up narrow channels and thin lakes. This can be obtained by first dilating the image, followed by eroding the result of the first operation.

The last morphological operation discussed here, is the majority operation. In this transformation one looks at for example the 8 neighbours of a single point and changes it to the value which agrees with the majority (here, 5 or more) of the neighbouring points.

4.2.3 Morphological operations performed

In order to generalize the obtained parameter values, the following procedure is used to reach the final result:

- Create a structuring element

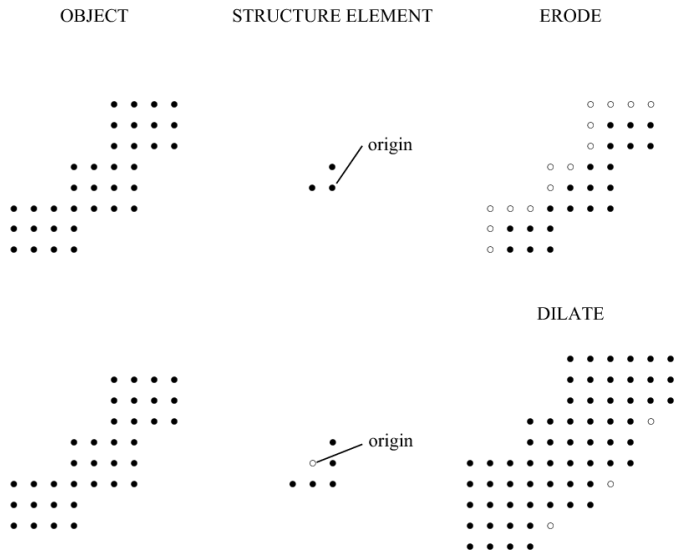

Figure 4.5: Erosion and dilation operations. Source:[7].

- Perform a closing operation
- Perform a erosion operation
- Remove areas smaller than 250 points
- Perform a majority operation

The procedure for this generalization is for both the amplitude and the wave length the same. The closing operation is performed in order to connect points with the same value, whereas the next erosion transformation corrects the enlargement of the former operation. Areas smaller than 250 points are removed, as uniform sand wave areas are assumed to be larger. Finally, the last operation is performed to smooth the results further.

The only difference in this generalization process between the amplitude and wave length is the size of the structuring element. In the amplitude case an element of 5×5 meter is used, while in the wave length procedure a 3×3 meter structuring element is created. This procedure is the outcome of an empirical trial and error method and seems to give a good, meaningful result. The difference in kernel size indicates that the amplitude classification is more disturbed compared with the wave length, which can also be seen in Figure 4.3. It explains the need for a larger structuring element in the amplitude generalization.

The generalized morphological parameter results are shown in Figure 4.6(a) and (b). To give an overview also the depth of the study area is classified. This result is rather easy obtained, as the depth is already completely spatial correlated and does not have to be categorized. The classification is obtained using the threshold values $Tr_d = (-12, -9, -6, -3, 0)$ and is shown in Figure 4.6(c).

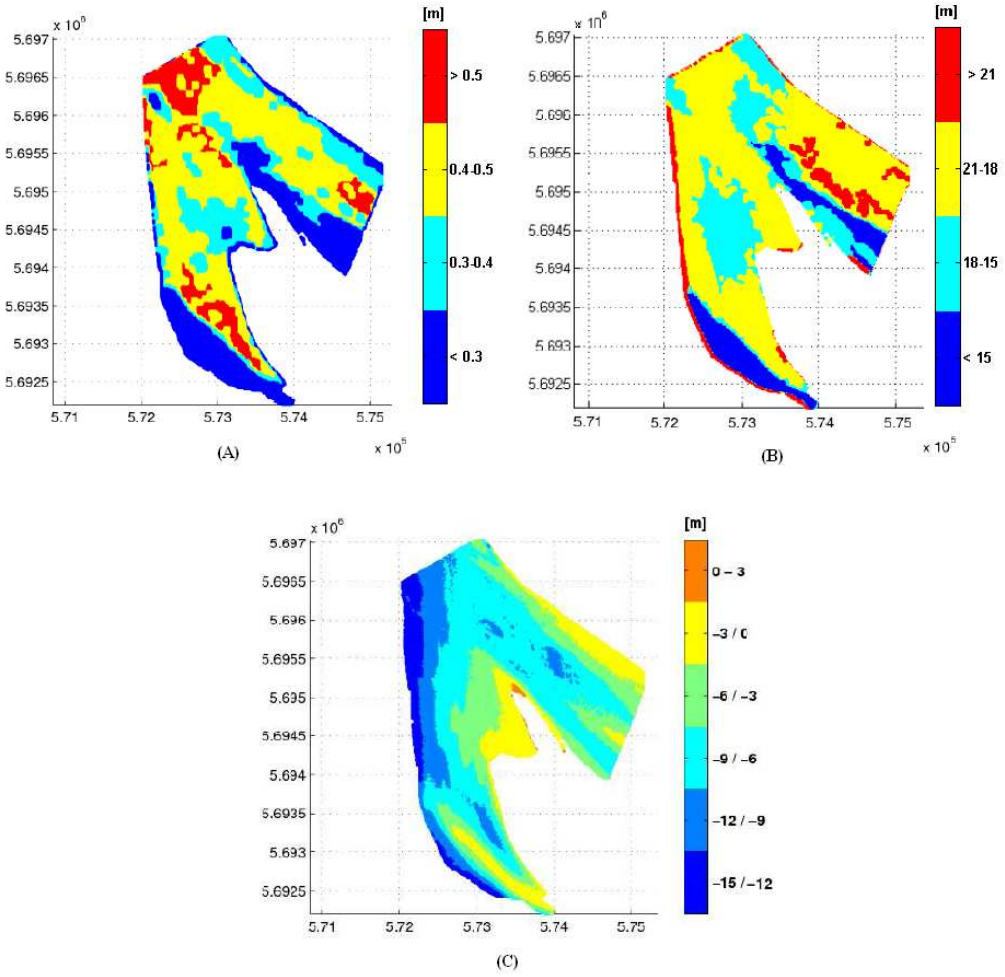

Figure 4.6: The results of the generalization procedure for the amplitude (A), wave length (B) and the depth (C).

Chapter 5

Area A: the sand dump

The disposal of 500.000 m^3 of sand is the primary reason for the sounding of time series of MBES measurements. In this chapter it is analyzed how the dumped sand is behaving. The area of the dump location near the shoal of Walsoorden will be discussed, considering the first two questions stated in Chapter 1. As strong changes can be expected, this region is of great interest.

In Section 5.1 the detection of the exact location of the sand dump will be described. The deformation, including the erosion and the distribution of the disposed sand, is discussed in Section 5.2. Finally, Section 5.3 gets into the morphological parameter changes of the bed forms.

5.1 Dump location

The region of the sand disposal has to be found in order to analyze this area extensively and to be able to answer the research questions stated in Chapter 1. The difference plots of the entire research area during the sand disposal moments give a first indication of the location of the sand dump. It can easily be seen from Figure 5.1 that in the sand dump period (i.e from t_1 until t_4) a certain region, North of the shoal of Walsoorden, has some abrupt deformation. This indication is affirmed by [12], stating that the sand was disposed at the seaward tip of the shoal of Walsoorden. Therefore it can be concluded that the area with abrupt deformation between t_0 and t_4 is very likely the dump location.

In order to define this area and obtain the data points involved, a stability test is performed. This test aims to discover whether or not a single point is stable over time. As the sand dump is executed in between t_0 and t_4 only these epochs are of interest for the determination of the area. For all the points it is assumed that the river floor was stable during the dump period. This leads to the following hypothesis:

$$H_0 : E\{ \begin{bmatrix} \underline{d}_{p_0} \\ \underline{d}_{p_1} \\ \underline{d}_{p_2} \\ \underline{d}_{p_3} \\ \underline{d}_{p_4} \end{bmatrix} \} = \begin{bmatrix} 1 \\ 1 \\ 1 \\ 1 \\ 1 \end{bmatrix} x_p \tag{5.1}$$

where d_{p_t} is the depth measurement on position p in epoch t and x_p is the estimated constant depth on position p.

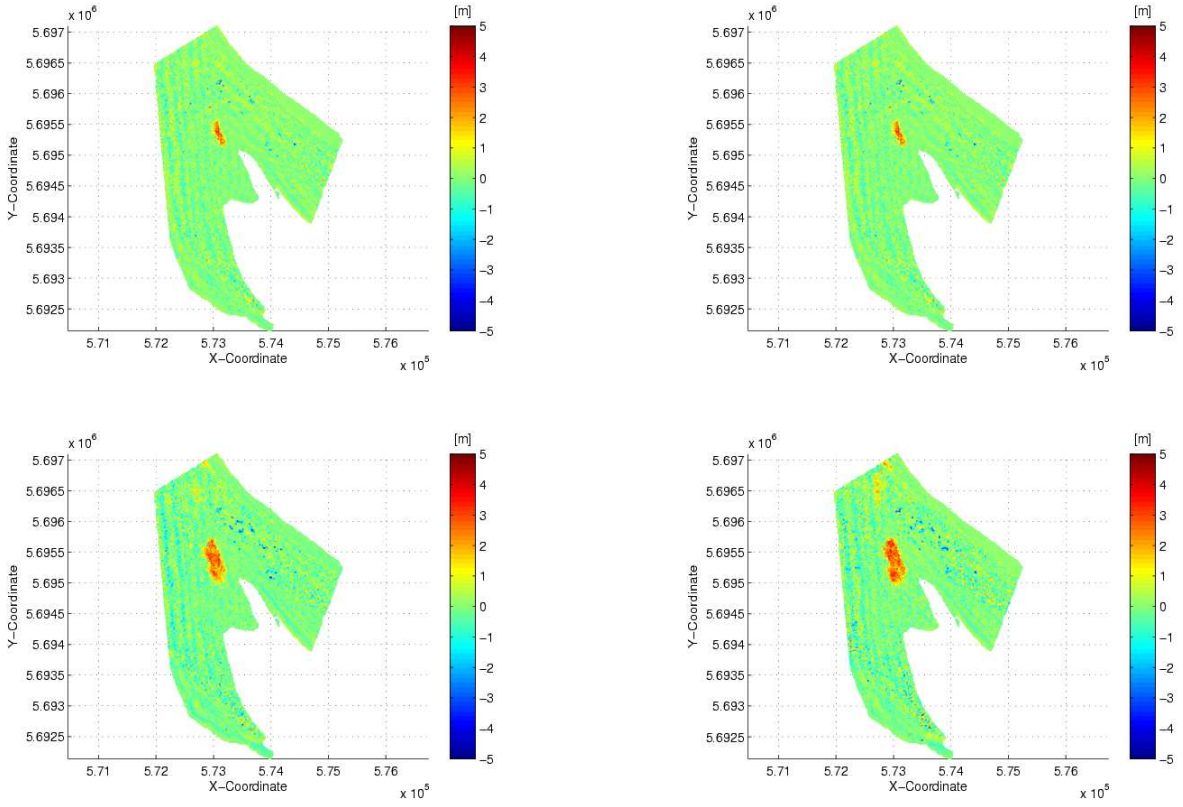

Figure 5.1: The difference of the research area at t_1, t_2, t_3 and t_4 with t_0.

The dispersion model of these measurements is very important in hypotheses testing as it influences the outcome of the test statistic significantly. Here, the correlation between observations in different epochs is assumed to be absent and a variance-covariance matrix is chosen with a relative large variance on the diagonals and zeros elsewhere:

$$D\{\begin{bmatrix} \underline{d}_{p_0} \\ \underline{d}_{p_1} \\ \underline{d}_{p_2} \\ \underline{d}_{p_3} \\ \underline{d}_{p_4} \end{bmatrix}\} = \begin{bmatrix} \sigma^2 & 0 & 0 & 0 & 0 \\ 0 & \sigma^2 & 0 & 0 & 0 \\ 0 & 0 & \sigma^2 & 0 & 0 \\ 0 & 0 & 0 & \sigma^2 & 0 \\ 0 & 0 & 0 & 0 & \sigma^2 \end{bmatrix}, \quad \text{with } \sigma = 0.32 \text{ m} \tag{5.2}$$

The hypothesis of stability is tested on the original dataset. The filtering operation is not yet performed, because filtering the total survey region in more than one epoch causes computational problems. Furthermore, the goal is to detect the dump location in the estuary, which is also possible using the original data points. However, as a consequence the value of the standard deviation σ has to be rather large. The reason for this is the presence of sand dunes. As mentioned in Chapter 2 the Western Scheldt has a very dynamic bottom, as it is covered with specific moving structures. These subaqueous dunes have a large influence on the deformation analysis and consequently on the stability hypothesis. Because of the fact that the dunes are constantly moving, one knows in advance that no single point is stable and therefore the hypothesis is false. By increasing the value of σ one is less strict in the difference between the

motion of the points and the proposed model. In practice this means that despite the moving sand dunes most of the stable points follow the hypothesis. Now, only the points containing large movements are rejected by the test. These locations are of main interest because they may belong to the dump location.

Hence, for this stability hypothesis testing, the bed forms act as noise. In Chapter 4 it is shown that the area where abrupt deformation takes place in between the first five epochs has bed forms with an estimated amplitude between 0.4 and 0.5 meters (see Figure 4.6). If the sand dunes are idealized by a sine function with an amplitude of 0.4 meters, the standard deviation of this function can be calculated, using:

$$\text{dune} = 0.4 \cdot \sin(x) \Rightarrow \sigma_{dune} = \sqrt{\frac{1}{n-1}\sum_{i=1}^{n}(y_i - m)} = 0.28 \text{ m} \tag{5.3}$$

with x the position, m the mean of all the samples from y and i the number of samples from the sine function. The calculated σ_y indicates the standard deviation caused by the sand dunes. The MBES surveys have a measurement inaccuracy and therefore do also have a standard deviation. In this study a σ_{meas} of 0.15 m is assumed. As no correlation between these standard deviations occur, the total σ can be computed, using the propagation law of variances (Eq 3.33):

$$\sigma_{total} = \sqrt{\sigma_{dune}^2 + \sigma_{meas}^2} = \sqrt{0.28^2 + 0.15^2} = 0.32 \text{ m} \tag{5.4}$$

The calculated standard deviation is necessary in the stochastic model of the stability hypothesis. Its value can be found in Eq. 5.2.

In order to test the validity of this stability model, one calculates for each point in the investigated area the test statistic $\underline{T}_q$ (Eq. 3.24) of the Overall Model test. Figure 5.2(a) demonstrates

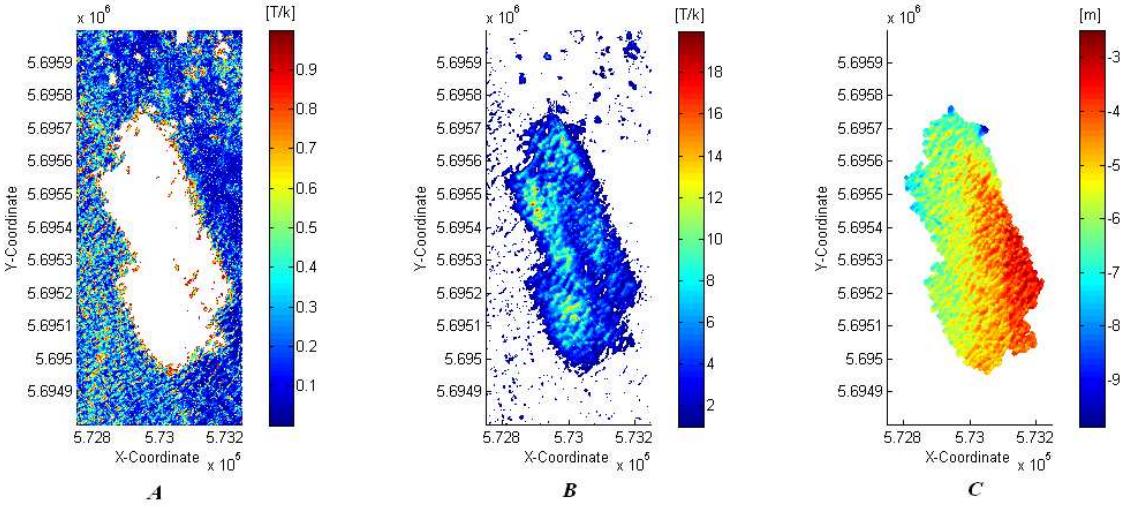

Figure 5.2: The test statistic of the accepted (a) and rejected (b) points by testing the stability hypothesis and the points which belong to the dump location (c).

this test statistic for the accepted points. A lot of rejected points, with a testing quotient above one (see Eq. 3.21), show clearly spatial correlation. At these locations the depth is not stable

between t_0 and t_4. Obviously, one expects this correlation at the sand dump location. Therefore, these unstable spatial correlated points are assumed to belong to the dump area. However, as can be seen in Figure 5.2(b), a lot of spatially uncorrelated points also rejected the stability hypothesis. This deformation is probably caused by the presence of the sand dunes in the estuary. In order to determine the sand dump location the spatial uncorrelated points need to be filtered out. Therefore, the requirement is stated that points belong to the dump location if one of the neighbours is also unstable and the region of unstable connected points to which it belongs, is the largest in the area wherefore the test statistic is calculated. The holes in this area are also considered as dump positions. This results in a clearly defined location which can be seen in Figure 5.2(c) as the points of the dump area at t_0.

5.2 Deformation analysis

After the determination of the research area, one wants to investigate how the Western Scheldt bed near the sand dump location changes over time. The erosion of the sand dump and its distribution elsewhere need to be considered. Therefore, it is necessary to perform a more sophisticated deformation analysis and test whether a model with a certain movement over time is a correct description of reality. However, in the Western Scheldt this is rather complicated as the estuary is covered with moving sand dunes. As the points are not measured with a constant time interval, the movement of the points, caused by the dunes, is very difficult to estimate. The bed forms will also cause large disturbances in the normal deformation analysis with models of stability, constant velocity and constant acceleration, unless the sand waves are modeled or filtered out.

Modeling sand waves is a very complex and difficult task. Especially if, as in the Western Scheldt, the bed forms do not have a uniform wave length, amplitude and orientation. Therefore, insight will be gained from filtering the waves out of the data. The method described in Section 3.1 is used to smooth the data and separate the sand waves from the topography. In Figure 5.3 results of the low pass filter operation are shown. These are performed with a kernel containing equal coefficients and a size of respectively, 5×5, 10×10, 20×20 and 25×25 pixels. It is clearly demonstrated that an increasing kernel size causes a smoother geography. The last plots (20×20 and 25×25) are rather smooth, while in the first two one can still see a lot of bed forms.

The kernel size gives an indication about the wave length of the sand dunes. In the ideal case, the low pass filter will separate the waves and topography completely. If all the points of a certain wave are taken into account by the convolution kernel, the filter operation will come closest to this ideal situation. Subsequently, a first assumption of the wave length value is about 25 meters, as with this kernel size the original data is divided rather well in topography and bed forms.

After the filter operation is executed, one is able to analyze the possible deformation of the sand dump location after the disposal. The first step is to perform a stability analysis and test whether or not the depths are changing at all. Only the epochs after the disposal, thus between t_5 and t_{16}, are of interest, because one knows in advance that in the first 5 epochs the dump

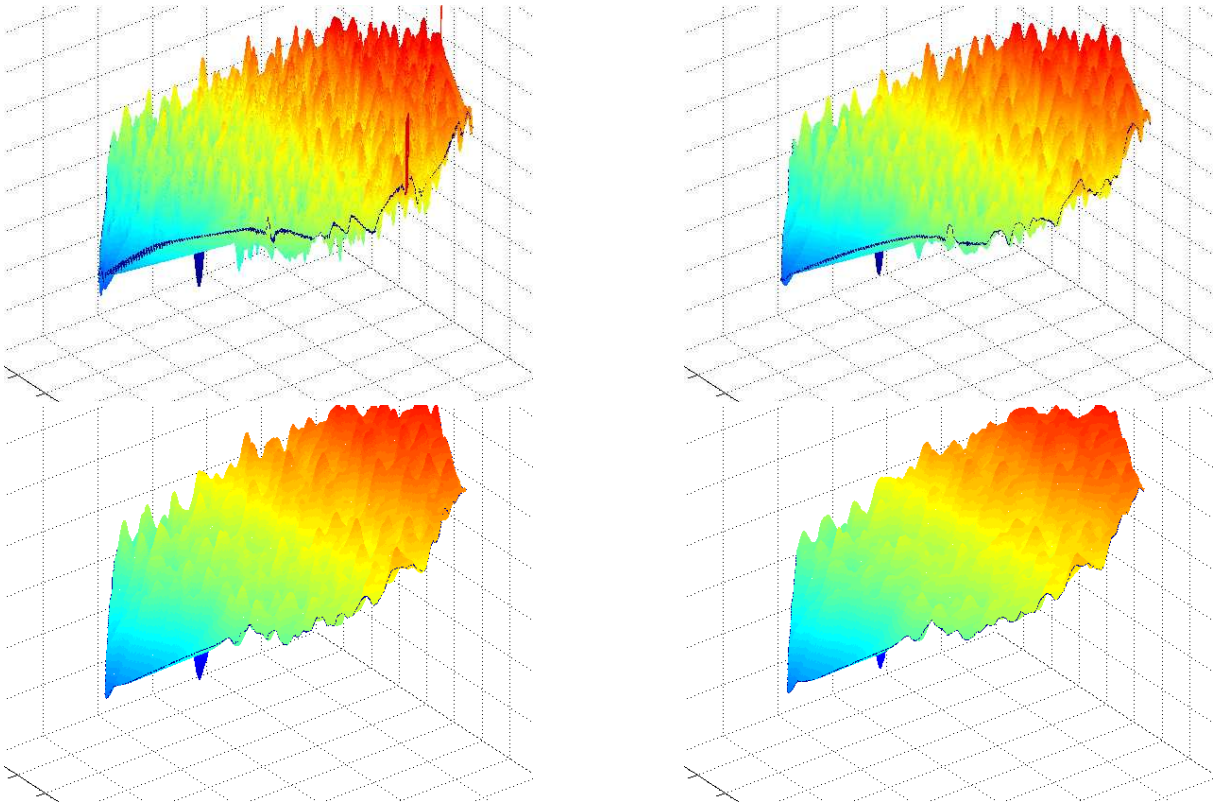

Figure 5.3: The filtering operation with kernels of 5×5 (upper left), 10×10 (upper right), 20×20 (lower left) and 25×25 (lower right).

location is not stable. Hence, the hypothesis is formulated as:

$$H_0 : E\{\begin{bmatrix} \underline{d}_{p_5} \\ \vdots \\ \underline{d}_{p_{16}} \end{bmatrix}\} = \begin{bmatrix} 1 \\ \vdots \\ 1 \end{bmatrix} x_p \tag{5.5}$$

with d_{p_t} the measured depth of position p in epoch t and x_p the estimated depth on position p.

The test statistic of the overall model test (Eq. 3.24) is calculated. By testing the stability hypothesis against the most relaxed hypothesis, one gets an indication whether the model is a good description of reality. The points which accept this test are assumed to be stable and are shown in Figure 5.4. Mostly, the quite shallow points in the south east of the dump area are considered stable.

However, a lot of points reject the stability hypothesis, which expresses the need for another model. Therefore, the hypothesis is extended toward a constant velocity model. It can also be seen as an increase of the time degree in the polynomial model (Eq. 3.25). Let t be the time in days, x_p the estimated initial depth and v_p the constant velocity of position p. Then, the hypothesis of constant velocity reads:

$$H_0 : E\{\begin{bmatrix} \underline{d}_{p_5} \\ \vdots \\ \underline{d}_{p_{16}} \end{bmatrix}\} = \begin{bmatrix} 1 & t_5 \\ \vdots & \vdots \\ 1 & t_{16} \end{bmatrix} \begin{bmatrix} x_p \\ v_p \end{bmatrix} \tag{5.6}$$

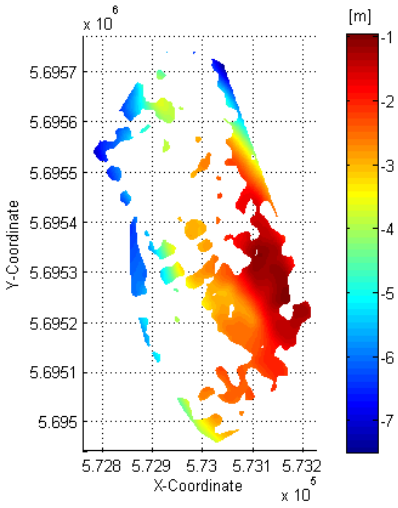

Figure 5.4: The depth of the points following the stability hypothesis.

Again, as in the stability case, this null hypothesis is tested first for overall validity in order to investigate whether or not this model is a good description of reality. A lot of points accept this hypothesis, which indicates that this model is able to describe the dynamics of the sand dump location. A small part of them also accepts the stability hypothesis of the first test. In order to solve this classification problem, the constant velocity hypothesis (Eq. 5.6) can be seen as an extension of the stability hypothesis (Eq. 5.5). The constant velocity hypothesis will now be treated as alternative hypothesis. Subsequently, the stability hypothesis is tested against the constant velocity hypothesis to check whether or not the extension is significant. The testing quotient $\underline{T}_q$ now has a χ^2 distribution with just one degree of freedom where in the overall model test of the stability hypothesis, it has $m - n = 11$ degrees of freedom, with $m = 12$ the number of observations and $n = 1$ the number of estimated parameters.

The result, plotted in Figure 5.5, shows a lot of points accepting the constant velocity model. One can clearly see a separation between the points with a negative (erosion locations) and a positive (deposition locations) velocity. Some disposed sand is obviously moving toward the shoal of Walsoorden, as also is concluded by [12].

Finally, the last formulated null hypothesis is again an increase in the time degree of the polynomial model, leading to the constant acceleration hypothesis:

$$H_0 : E\{\begin{bmatrix} \underline{d}_{p_5} \\ \vdots \\ \underline{d}_{p_{16}} \end{bmatrix}\} = \begin{bmatrix} 1 & t_5 & \frac{1}{2}t_5^2 \\ \vdots & \vdots & \vdots \\ 1 & t_{16} & \frac{1}{2}t_{16}^2 \end{bmatrix} \begin{bmatrix} x_p \\ v_p \\ a_p \end{bmatrix} \tag{5.7}$$

with x_p the initial reference depth, v_p the constant velocity and a_p the constant acceleration of point p.

Exactly the same procedure as in the constant velocity case is followed to determine which points belong to this model. After the overall model test, the hypothesis of constant velocity is tested against this constant acceleration model, to check the significance of this extension. The results, shown in Figure 5.6, can indicate for the accepted points a decrease in erosion and

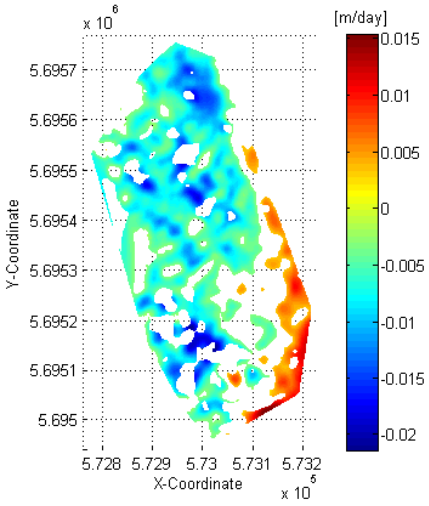

Figure 5.5: The velocity of the points following the constant velocity hypothesis.

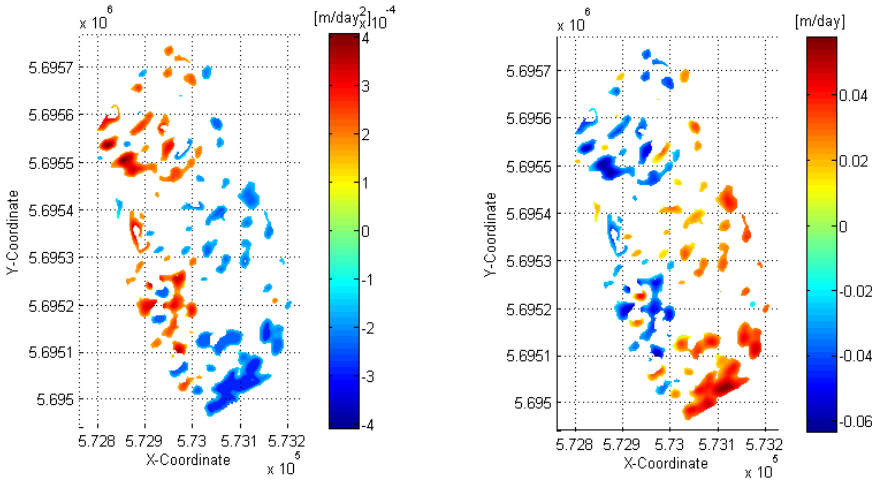

Figure 5.6: The points following the hypothesis of constant acceleration, with the acceleration (left) and the velocity (right) estimations.

deposition speed. The negative acceleration combined with a positive speed, shown mostly for the points in the south of the dump area, can represent a decrease of the deposition speed in the last epochs, whereas the positive acceleration with a negative speed may indicates a reduction of the erosion speed, mainly located in the northern part. Intuitively, this model can be a good description of the dynamics of a point. One can easily understand that directly after the sand dump the changes are larger than between the last couple of sounding moments. The amount of eroded or deposited sand coming from the dredged material is at that time already in its place and the depth stabilizes. These changes are visualized in Figure 5.7 for a deposition and an eroded point.

88,3% of the points are accepted by one of the three models. The amount and percentages of the points following a certain hypothesis are shown in Table 5.1. It demonstrates that the change of by far the most points can be described by the model of constant velocity. A fur-

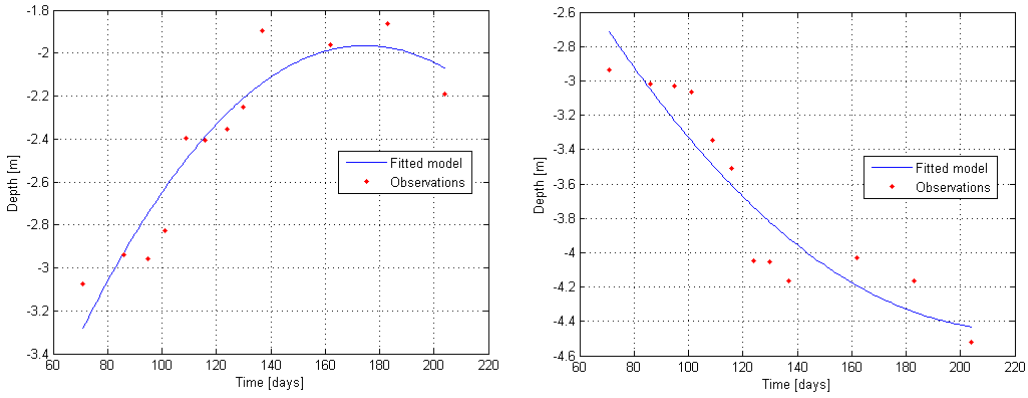

Figure 5.7: A profile of a deposition point (left) and a eroded point (right).

ther extension of the models does not lead to a hypothesis with a significant number of accepted points. A visual inspection indicates that for the rejected points the separation of the sand dunes and coarse topography was not ideal, which causes the rejection of all the three hypotheses.

	Stability	*Constant velocity*	*Constant acceleration*	*None*
Points	16.397	159.233	12.947	24.953
Percentage	7,7%	74,5%	6,1%	11,7%

Table 5.1: The amount of points and percentages following a certain hypothesis.

Distribution of the dumped sand

The acceptance of hypotheses of constant velocity and acceleration by most of the points show an erosion of the sand dump. The positive velocity in Figure 5.5 and Figure 5.6 indicate a movement of the disposed sand in South-East direction. As also its distribution outside the disposal region is of great interest, the area for the hypothesis testing is extended. In Figure 5.8 the results of the deformation analysis are shown, giving an overview of the dump erosion. The outline represents the sand dump location. On the bottom right, the most Northern point of the shoal of Walsoorden is visible where echo sounding was not possible. Gray points are tested stable. At yellow to red points, siltation occurred at an average rate of up to 1.5 cm a day. Erosion occurred for the green points of up to 2 cm a day. It can be seen clearly that the dumped sand is moving in the direction of the shoal of Walsoorden.

As stated in Chapter 3, the acceptance of a hypothesis depends on several values that can be assumed or calculated. In the testing procedure of these hypotheses, a level of significance α of 0.005 is chosen. The standard deviation for the original data is based on the measurement inaccuracy of the multi-beam echo sounder and the presence and amplitude of the sand dunes (Eq. 5.4). For the deformation analysis after the sand disposal, the filtered data is used. As a consequence, the σ_{dune} equals zero in the case the filtering procedure is ideal. Then, σ_{total} equals σ_{meas}. Unfortunately, the *low pass filter* is not a perfect and therefore in principle the σ_{dune} is not zero. However, this term is that small that it does not have a large influence in the stochastic model, which belongs to the models in the last three hypotheses. Hence, a standard

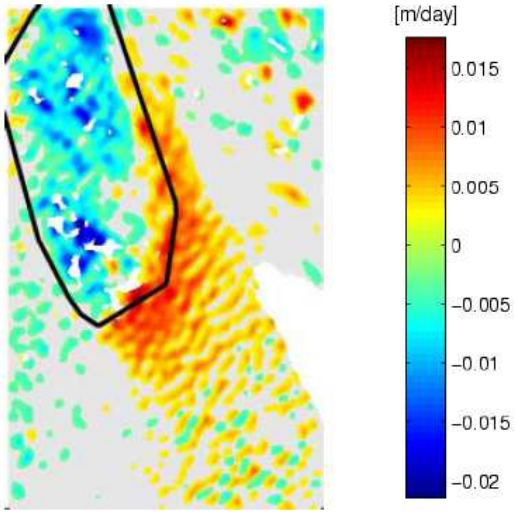

Figure 5.8: The deformation of the sand dump in an extended area.

deviation equal to the assumed measurement inaccuracy is used, leading to:

$$D\{\underline{d}\} = 0.15^2 I \tag{5.8}$$

Volume change

One can conclude from the deformation analysis that by far most of the points follow the constant velocity hypothesis. This indicates that the disposed sand is partly eroding toward the shoal of Walsoorden. The amount of sand moved out of the dump location, can be calculated by multiplying the deformation speed and acceleration, the time difference ΔT between t_5 and t_{16} and the surface area:

$$E_{cv} = (v_{e_{cv}} \Delta T) S_{e_{cv}} \tag{5.9}$$

$$D_{cv} = (v_{d_{cv}} \Delta T) S_{d_{cv}} \tag{5.10}$$

$$E_{ca} = (\frac{1}{2} a_{e_{ca}} \Delta T^2 + v_{e_{ca}} \Delta T) S_{e_{ca}} \tag{5.11}$$

$$D_{ca} = (\frac{1}{2} a_{d_{ca}} \Delta T^2 + v_{d_{ca}} \Delta T) S_{d_{ca}} \tag{5.12}$$

$$M = E_{ca} + D_{ca} + E_{cv} + D_{cv} \tag{5.13}$$

with M the moved sand out of the area, E and D the total erosion and deposition of the points, following a certain hypothesis, cv the constant velocity hypothesis, and ca the constant acceleration hypothesis, v the mean velocity, a the mean acceleration and S the area surface of the points involved.

The result of this calculation leads to a decrease in volume of 115.690 m^3 in the disposal area, with a standard deviation $\sigma = 24.596$ m^3. This means that 23% of the 500.000 m^3 sand moved out of the dump area. The calculated erosion is compared with [12], who obtained a volume change of 74.877 m^3. The reason for this difference and the large standard deviation may be found in the fact that in our computation the amount of moved sand is calculated on the basis of a deformation model. This means that a deformation speed and acceleration are estimated

which not necessarily fit the value at t_{16} in the best possible way. The values are estimated in order to fit all the values in time. However, because [12] does not describe how his value is obtained, a comparison between the two values is impossible.

From the 115.690 m^3 eroded sand, a large part moves toward the shoal of Walsoorden. A volume calculation indicates that the amount of sand which can be found back in the south-east direction is 89.164 m^3. This represents a percentage of about 77 % of the eroded material.

5.3 Parameter analysis

Having detected the deformation of the global topography, of further interest is if and how fast bed forms will reappear on top of the sand dump. The parameters considered here are the wave length and the amplitude of the subaqueous sand dunes as a function of time.

As described in Section 3.1 the residuals of the filtering represent the sand dunes data only; the coarse topography is subtracted from the dataset. Thus, in order to determine the dune parameters, the residuals after the filter operation have to be analyzed. Use is made of two methods for parameter estimation described in Section 3.2, the *profile line based method* and the *directional variogram method*.

5.3.1 The profile line based method

The first method for determining the amplitude and the wave length of the sand dunes is by drawing profiles through the sand dune data. In this method there are two approaches, the so called classification method, which estimates for each grid point an own orientation, and the profile line method, which assumes one sand dune orientation for all the bed forms.

The classification method

The calculated amplitude and wave length of the grid points are not always the same. However, the region is assumed to be uniform. To indicate the strength of the obtained parameters, the standard deviation can be calculated. Using Eq. 3.3. a σ of 0.12 m for the amplitude and a σ of 4.12 m for the wave length are obtained. The large value for the standard deviation of the wave length is likely due to wrong identifications of the dune orientation. As can be seen in Figure 5.9 the histograms show a relative large number of points for which a deviation of the orientation is estimated.

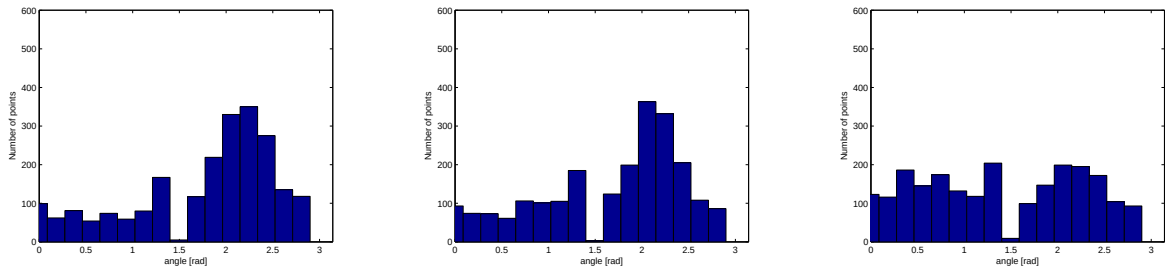

Figure 5.9: Histograms for the wave direction at t_0, t_7 and t_{16} for the dump location.

The results of the estimation are shown in Figure 5.10. One can clearly see that the amplitude is decreasing during the sand disposal period, which agrees with the expected disappearance of the sand dunes. Subsequently, the amplitude rises after the dump until the normal value is reached again. The sand dunes are reappeared. The wave length plot shows a slight increase in the parameter estimation a few meters. However after the sand dunes are reappeared the wave length stabilizes.

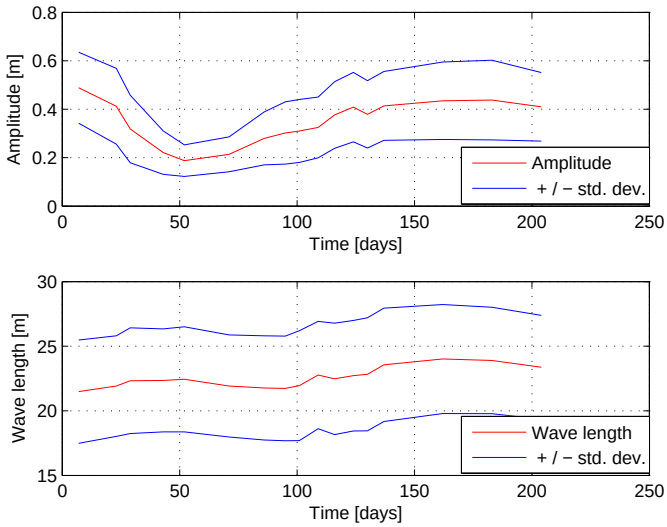

Figure 5.10: The amplitude and wave length over time, using the classification method.

The profile line method

In this approach one sand dune direction is used for drawing the profile lines. This direction is chosen by making use of the histograms of the classification method. Except this point, the method estimates in exactly the same way the amplitude and wave length of the bed forms.

As the amplitude and wave length differ along a certain profile, 100 different profiles are drawn in the sand dump region. The parameter values are assumed to be the same for the whole area. Therefore, the standard deviation of the parameters can be calculated using Eq. 3.3. This leads to a σ of 0.05 for the amplitude and a σ of 1.76 for the wave length.

The overall results are shown in Figure 5.11. Also using this method, a decrease in amplitude can be observed during the sand disposal period and reappears when t is about 140 days. The wave length plot shows an obvious growth of a few meters after the disposal and after about 150 days it seems to stabilize.

5.3.2 The variogram method

In the case of the Western Scheldt most directional variograms have a cyclical form. This has a physical interpretation and is due to the presence of sand dunes. As explained in Section 3.2 the parameters of interest can be estimated from the variograms.

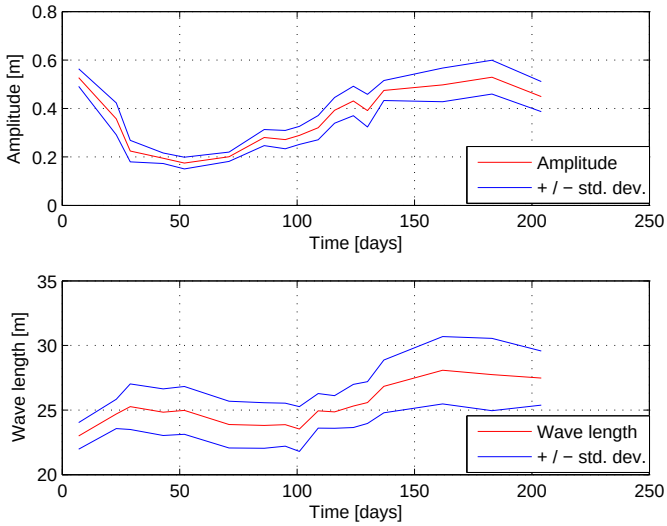

Figure 5.11: The amplitude and wave length over time, using the profile line method.

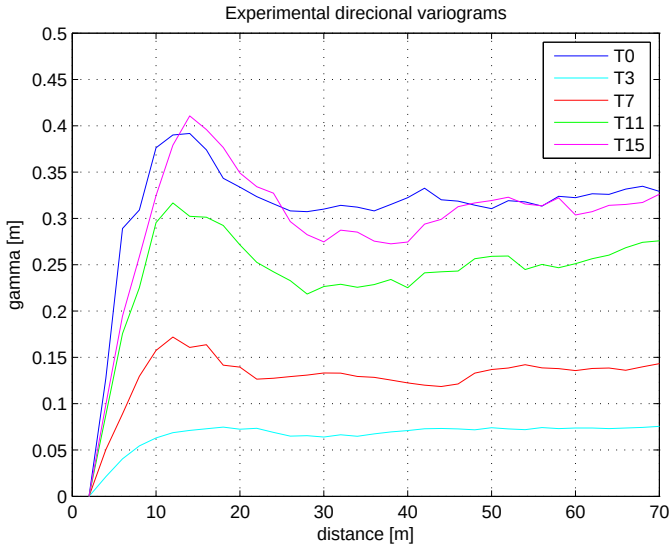

Figure 5.12: Five Directional experimental variograms.

The same orientation angle is chosen as for the profile line method to calculate the spatial variability. In Figure 5.12 the directional experimental variograms for the five epochs as indicated are shown. It demonstrates the variogram of the original sand dune t_0, before the sand dump took place and its development in time. Clearly the decrease of the amplitude of the sand dunes during the sand disposal (t_3) is shown. After this, one sees that the maximal variability, a measure for the amplitude, grows until it reaches a value in t_{15} where it equals again the first, pre-sand dump maximal variability (t_0). As stated before, the wave length can be determined by looking at the location of the first hole-effect. This distance and consequently the wave length seems to increase. During and immediately after the sand disposal the bed of the dump location is quite flat. This absence of the sand dunes can be seen in the variogram at t_3, where the hole

effect is disappeared.

The problem however is that the periodicity can not be determined clearly. As can be seen from Figure 5.12 it is rather difficult to estimate the distance toward the first hole unambiguously. Thus the wave length of the subaqueous sand dune is impossible to determine in a good way from the experimental variogram. The solution lies in fitting a continuous function, in this case an exponential Bessel function, through the experimental variogram:

$$\gamma(h) = c[1 - (\exp(\frac{-h}{a}))(J_0(b \cdot h))] \tag{5.14}$$

where h is the distance vector, c a scale factor, a is a damping factor and b is the frequency of the continuous variograms. J_0 is the Bessel function of order 0, which looks similar to a damping cosine function and is defined as [10]:

$$J_0(b \cdot h) = \sum_{m=0}^{\infty} \frac{(-1)^m (b \cdot h)^{2m}}{2^{2m}(m!)^2} = 1 - \frac{(b \cdot h)^2}{2^2(1!)^2} + \frac{(b \cdot h)^4}{2^4(2!)^2} - \frac{(b \cdot h)^6}{2^6(3!)^2} + - \cdots \tag{5.15}$$

If the optimal values for a, b and c can be estimated, a good continuous variogram can be fit through the experimental variogram. Hence, the wave length and the amplitude parameters can be determined as described in Section 3.2. The optimal estimations are performed for different epochs using the Kriging Toolbox [5]. Figure 5.13 shows the continuous variograms fitted through the experimental variogram. For this application, it is important that the continuous variogram fits good until the first hole effect occurs, because afterwards, the continuous function is not used any more for the calculation of the parameters.

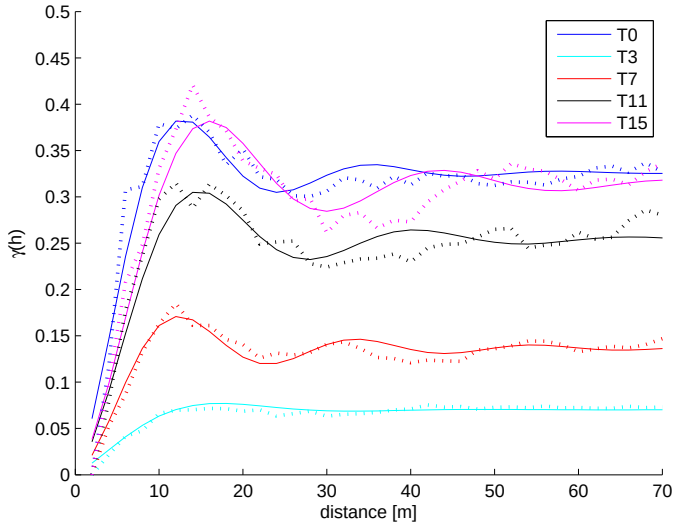

Figure 5.13: The continuous variograms (solid line) fitted through the experimental variograms (dotted line).

The estimated morphological parameters, obtained from the continuous variograms, are shown in Figure 5.14. It demonstrates that the amplitude decreases after the beginning of the disposal activities (the sand dunes disappear), but rises again until the original value is reached

after about 150 days. The wave length plot looks rather strange with large differences in the beginning. However, these odd values can be explained. The method for the calculation of this parameter is based on estimating the distance toward the first hole effect. Obviously, after the beginning of the disposal, the sand dunes are filled up with the dumped sand. A flat area means the absence of the hole effects in the variograms (as can also be seen in figure 5.12) and the estimation toward the first hole will be meaningless. Thus, this method for estimating the wave length does not give good results for the epochs where the sand dunes are disappeared. In the end, when the sand waves are reappearing the wave length seems to increase by a few meters, but stabilizes in the end.

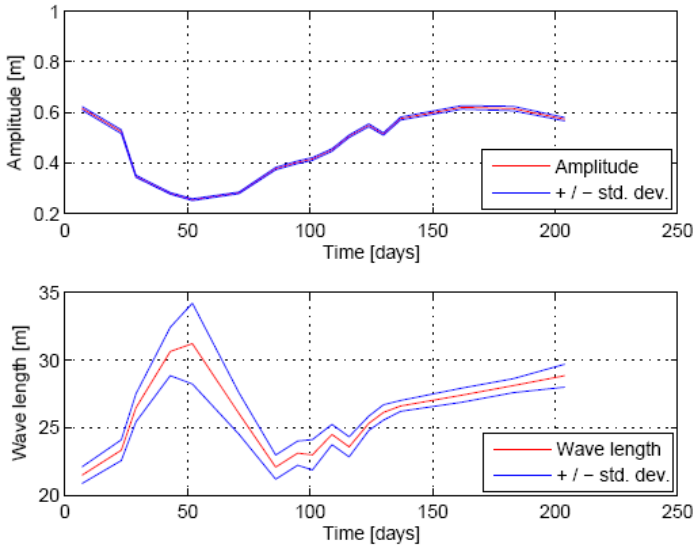

Figure 5.14: The amplitude and wave length over time, using the variogram method.

The variogram cloud is calculated for a subset of 10.000 points, as more points will cause calculation time problems. The standard deviation of the parameters can be estimated using the bootstrapping method (Eq. 3.6). This procedure is performed for $n = 100$, which means for 100 subsets the continuous variograms are calculated and subsequently the parameters are estimated. This leads to a mean σ for the amplitude of 0.006 m and a mean σ for the wave length of 0.97 m. However, the standard deviation of the amplitude is not a realistic number and thus the bootstrapping method can not be used for this parameter. Apparently, the maximal values of the continuous variograms are not strongly influenced by taking subsets. This can be explained, realizing that the amplitudes of the variograms are not that indistinct as in the case of the wave lengths. In the experimental variogram the distance until the first hole effect is much more difficult to determine than the maximal value.

5.3.3 Concluding remarks

Two different approaches are used for the determination of the sand dune parameters. A comparison between the two methods is made using Figure 5.15, the results of the both techniques in one plot. The two different methods are quite similar if one looks at the amplitude. Although Figure 5.15 shows a small translation, the trend is exactly the same. Even the small jump after

130 days is visual in both results. The similarity of the results indicates that the methods are working and gives confidence in the outcome. The conclusion can be stated that the amplitude decreases after the beginning of the disposal activities (the sand dunes disappear), but rise until the original value in about 150 days.

In contrast with the amplitude the wave length plots differ a lot. However, it is already mentioned that the variogram method does not work for the estimation of the wave lengths when the dunes are filled up with disposed sand. Thus, for this method only the values after about 100 days have to be taken into account. Subsequently, one sees in both methods an increase in the wave length. The trend looks quite similar, which gives us again confidence in the results.

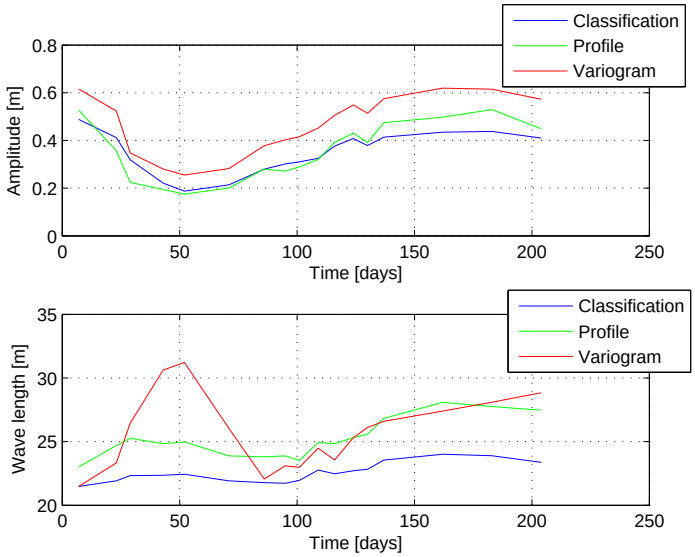

Figure 5.15: The amplitude and wave length over time, estimated with the three different methods.

The overall conclusion that can be drawn is the return of the pre-sand dump amplitude size after about 150 days. It seems that the depth of the area does not influence the size. The wave length, however, is a different story. It increases a few meters after the disposal and seems to stabilize in the end. Here the actual bottom depth may play an important role, but also the different properties of the dumped sand can be the cause.

However, it is concluded that all the three methods give the same trend, but not in the same range. This discrepancy can appear on account of three different reasons:

- *The natural variability is not filtered out*
  The maximal variogram value is used for the estimation of the amplitude. However, the normal variability at the distance of the peak is not taken into account. Therefore, the variability caused by the sand waves is overestimated, leading to a larger amplitude.

- *A local extreme is wrongly defined*
  In the profile line method assumptions have to be made in order to define a local extreme. In these methods a local extreme is detected if and only if it is the center point of a local profile of 25 meters has an extreme value. This means that a wave length smaller than

half the profile line, i.e. 13 meters can not be detected. However, this demand may be too strict, with the consequence that some extremes may not be detected.

- *The wave direction is not stable over time*
  In the variogram and profile line method a constant wave direction over time is assumed. However, as the histograms in Figure 5.9 demonstrate, the wave direction differs over time. As a consequence the wave length in the variogram and profile line method can be estimated too large. Especially in the last two epochs, with a lot of non-uniform wave directions, this can be the case.

Chapter 6

Area B

After the analysis of the changes in the disposal region, a second, more stable area is investigated in this chapter. The determination of the sand dune parameters as a function of time is emphasized, more than the deformation. By examining also the evolution of these parameter values in this second area, one can get more insight in changes which are not directly caused by the sand dump.

The same approach as in Chapter 5 is followed. Section 6.1 deals with the determination of the area, the deformation analysis will be discussed in Section 6.2, whereas Section 6.3 focuses on the morphological parameters.

6.1 Determination area

First of all, a suitable area has to be chosen. The objective is to find a homogeneous part of the area, with uniform amplitude and wave lengths. This simplifies the detection of parameter changes significantly. As the sand dump was performed on a more shallow area, in this new case also a deeper part was preferred.

The area can be selected with the help of the classification process, performed in Chapter 4. As one can see in Figure 4.6(a), a quite large area north of the shoal of Walsoorden seems to have a uniform, rather large wave length. Figure 4.6(b) demonstrates that this region also has a uniform wave length at t_0, whereas in Figure 4.6(c) it can easily be seen that the area is significantly deeper than the region where the sand is disposed. Thus, being able to meet all the requirements, this area north of the shoal of Walsoorden, shown in Figure 6.1, is selected for further research.

6.2 Deformation analysis

A deformation analysis is performed to be assured that the selected area does not alter much and no sand dump has taken place. The models tested on the data points are the same as those described in Chapter 5, but in this region the observations of all the 17 epochs are used to test the hypotheses, leading to:

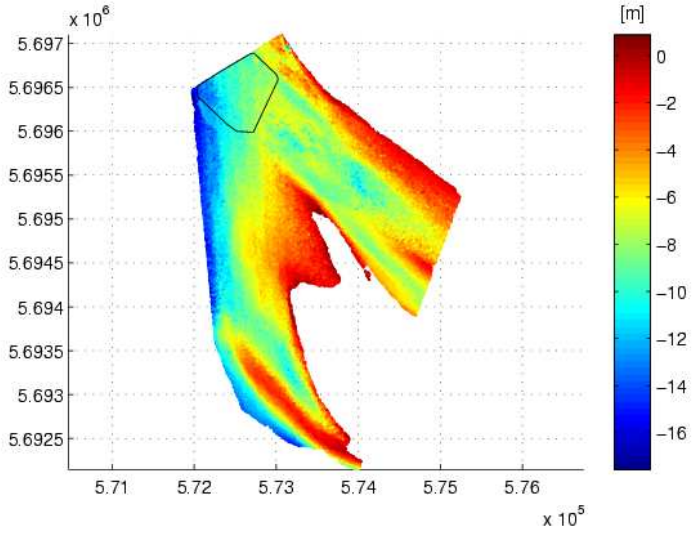

Figure 6.1: Area B outlined in the total study area.

- The model of stability:

$$H_0 : E\{\begin{bmatrix} \underline{d}_{p_0} \\ \vdots \\ \underline{d}_{p_{16}} \end{bmatrix}\} = \begin{bmatrix} 1 \\ \vdots \\ 1 \end{bmatrix} x_p \tag{6.1}$$

- The model of constant velocity:

$$H_0 : E\{\begin{bmatrix} \underline{d}_{p_0} \\ \vdots \\ \underline{d}_{p_{16}} \end{bmatrix}\} = \begin{bmatrix} 1 & t_0 \\ \vdots & \vdots \\ 1 & t_{16} \end{bmatrix} \begin{bmatrix} x_p \\ v_p \end{bmatrix} \tag{6.2}$$

- The model of constant acceleration:

$$H_0 : E\{\begin{bmatrix} \underline{d}_{p_0} \\ \vdots \\ \underline{d}_{p_{16}} \end{bmatrix}\} = \begin{bmatrix} 1 & t_0 & \frac{1}{2}t_0^2 \\ \vdots & \vdots & \vdots \\ 1 & t_{16} & \frac{1}{2}t_{16}^2 \end{bmatrix} \begin{bmatrix} x_p \\ v_p \\ a_p \end{bmatrix} \tag{6.3}$$

Thus, the models of constant stable points, constant velocity and constant acceleration are tested, which yields to the results shown in Figure 6.2. It demonstrates in one plot the points accepting the hypothesis of a constant acceleration, constant velocity or stability. Clearly, some changes take place in the eastern part of the selected area. These deformations are possibly caused by a sand dump, as a sudden change in height is found. As a stable area is wanted for the parameter analysis, the study area is further reduced to the western part. The detected deformation in this region is likely due to the fact that the sand wave filtering is not optimal.

6.3 Parameter analysis

For the reduced area the morphological parameters of the sand waves are estimated for each epoch. Assuming that the wave length and amplitude are uniform one can determine one single

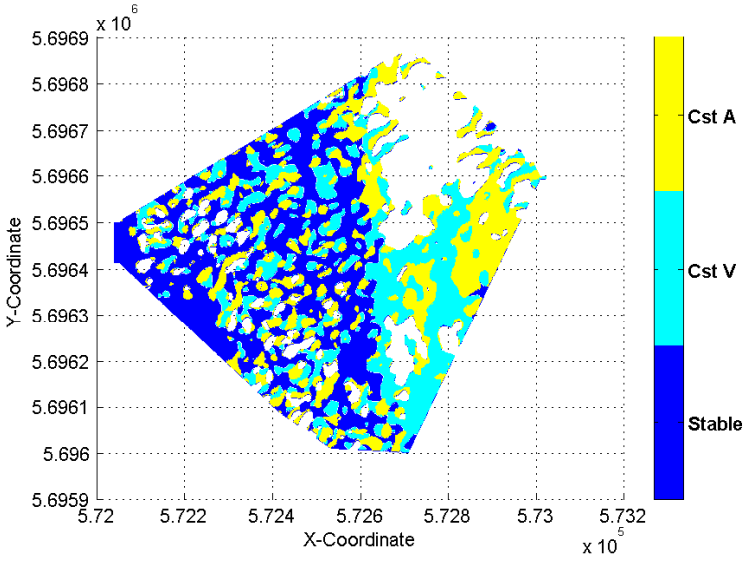

Figure 6.2: The accepted points of the three hypotheses.

value for the whole area. Two different methods are used to estimate those parameters:

- The profile line based method
- The variogram method

These methods will be used again to be able to compare the different results, and give insight in the changes of the morphology.

6.3.1 The profile line based method

The classification method

In the procedure of this method first the sand wave direction is estimated and subsequently the wave length and amplitude are obtained by considering the number and heights of the local extremes. As a result, each point is provided with amplitude and wave length information and the mean and the variance of these parameters are calculated as well. This leads for this new area to the estimated parameters, as can be seen in Figure 6.3. Except for a sudden decrease in amplitude after 29 days and a small feature after 124 days, it seems rather stable. The wave length shows also some strange features on the same time moments, but has a certain positive trend in the beginning and stabilizes in the end. The mean σ obtained for the amplitude is 0.13 m and for the wave length 2.7 m.

In determining the area, the objective was to select a homogeneous region with a uniform wave length, amplitude and direction. Whereas the uniformity of the first two is indicated by the variance, the homogeneity of the direction can be demonstrated by the spread in the histograms of the obtained direction. Figure 6.4 shows these histograms, indicating an almost perfect normal distribution at the first sounding moment at $t = 7$. This indicates a uniform, homogeneous wave orientation. After $t = 7$ the number of point with the original orientation is decreasing in time. Especially in the last two epochs the dune direction is rather indistinct. However, the original dominating wave direction stays visible.

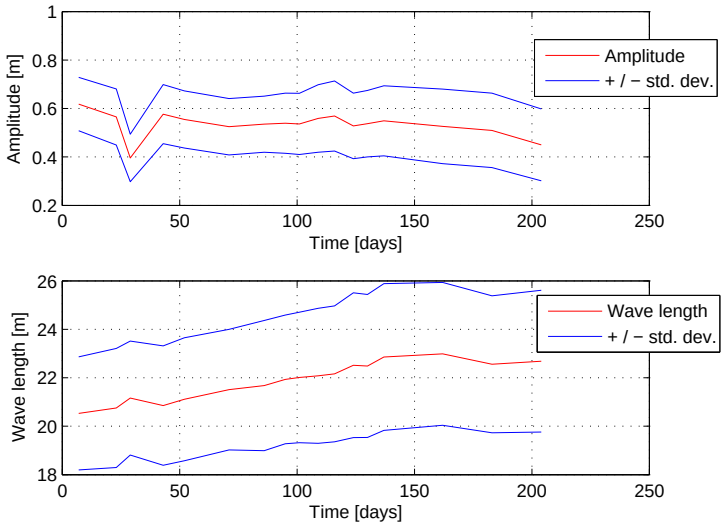

Figure 6.3: The amplitude and wave length over time, using the classification method.

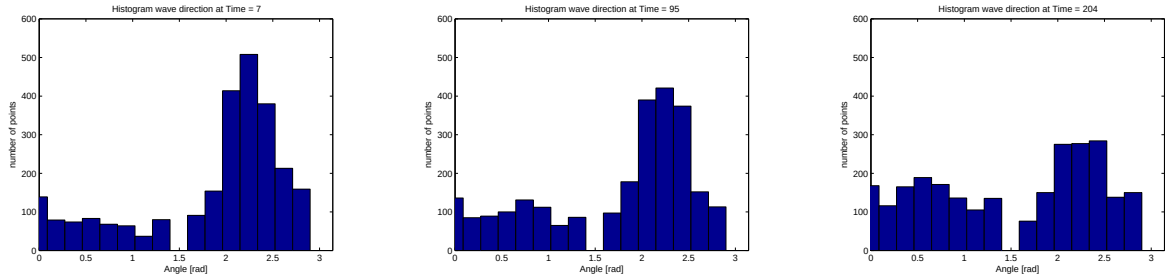

Figure 6.4: Histograms for the wave direction at t_0, t_7 and t_{16} days.

Profile line method

The profile line method works in principle the same as the classification method, but it is distinguished by the fact that the wave direction in this method is not estimated but chosen. This gives the advantage that for each point the same direction is used, leading to significant larger profile lines. Performing this operation in this new area, the mean wave length and amplitude are shown in Figure 6.5. It demonstrates an abrupt change in the amplitude at $t = 29$ and a much smaller decrease at $t = 124$. The wave length plot shows a sudden increase at $t = 29$, disturbing the constant trend over time. The mean of the standard deviation σ is calculated using Eq. 3.3 which leads for the amplitude to 0.05 m and for the wave length to 2.42 m.

6.3.2 The variogram method

In the variogram method, one first obtains experimental variograms. Then, a continue function is estimated through these points and as this function describes a hole effect, the distance to the hole and and the maximum value can be estimated, leading to wave length and amplitude information. Figure 6.6 shows the results of this method. The amplitude diminishes heavily at $t = 29$ and also a reduction is seen at $t = 124$. The wave length plot demonstrates a constant

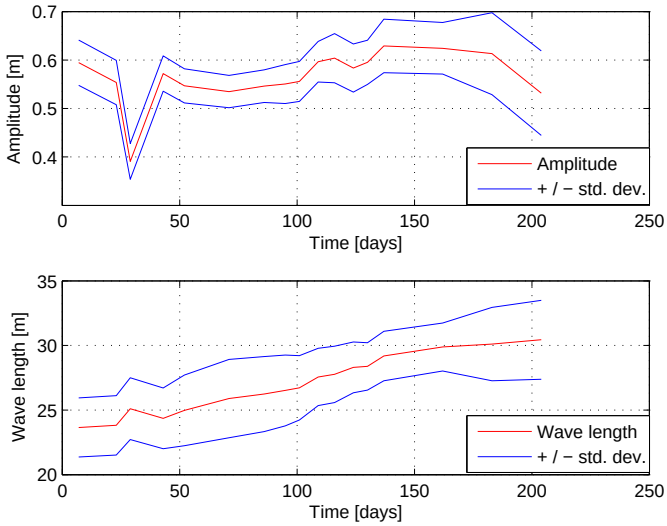

Figure 6.5: The amplitude and wave length over time, using the profile line method.

trend, except at $t = 29$ where an abrupt peak can be seen. The quality of the method can be described with the standard deviation σ. By calculating this value, use is made of the fact that the variogram cloud is made with a subset of the data, in order to avoid calculation problems. The continuous variogram is estimated 100 times, using each time a different, randomly chosen subset. The standard deviation is obtained using Eq. 3.6, leading to a mean σ for the wave length of 0.7. However it must be mentioned that the σ at $t = 29$ is with a value of 2.6 m exceptionally high. For the amplitude the mean σ is 0.014.

6.3.3 Concluding remarks

Combining all these estimation methods, one can compare the results. In Figure 6.7 it can clearly be seen that all the three methods give the same trend, but not in the same range. This discrepancy can appear on account of three different reasons. Those are already mentioned in Section 5.3 and consider the *normal variability*, the *wrongly defined extrema* and the *not stable wave direction over time*.

However, one of the objectives is to investigate whether or not there is a relation between the parameter changes and the meteorological and tidal data. For this purpose, the absolute values are not the most important, but the relative changes are of interest.

One can clearly see a sudden amplitude change in all three the methods at $t = 29$. Also at $t = 124$ a small distortion has taken place, but in general the amplitude seems stable. For the wave length, there is a general positive trend over time. However, at $t = 29$ there appears a sudden increase in all three the methods. The rise is the most extreme in the variogram method, but its σ is quite large at this epoch as well.

It is very important that the results of the three methods correspond with each other. Also all the remarkable features are found in the results of each method. As the approach is completely different, this gives high confidence in the outcome.

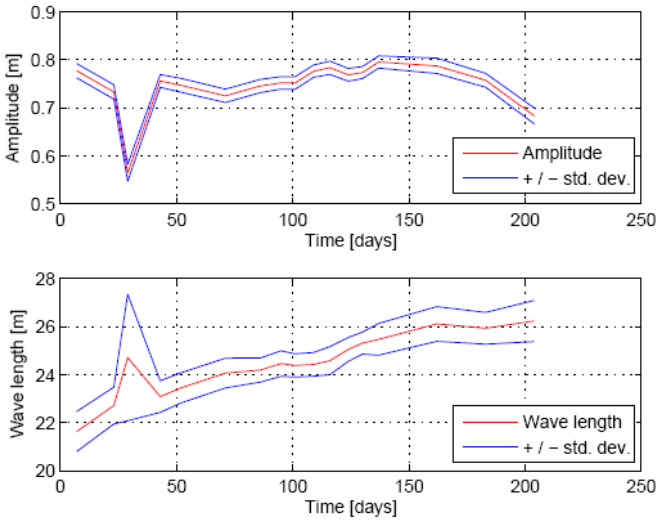

Figure 6.6: The amplitude and wave length over time, using the variogram method.

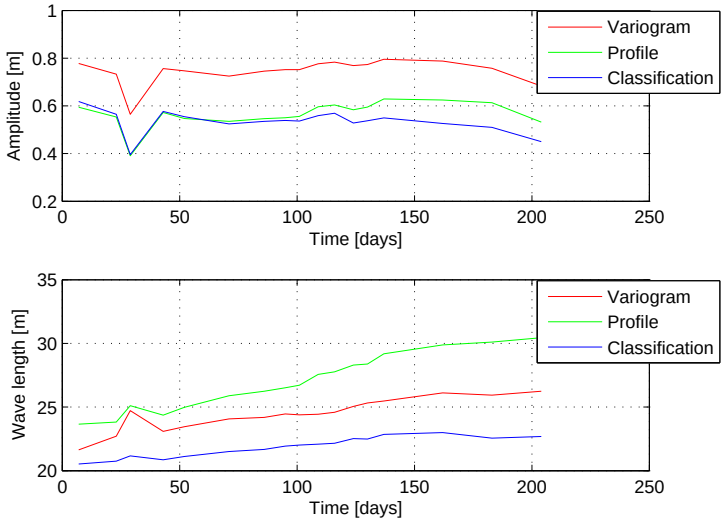

Figure 6.7: The amplitude and wave length over time, using three different methods.

Chapter 7

Relation between dune parameters, weather conditions and tides

In Chapter 3 it is explained how to obtain subqueous and dune dune parameters as a function of time. In order to understand and explain their changes over time, one can investigate possible relationships between the change pattern and other physical parameters. Correlation analysis can reveal a relation between different variables and gives insight in its strength. However, when a *statistical* correlation is discovered this does not automatically mean that there exists a *causal* connection.

In Section 7.1 two techniques applied to investigate whether there is a linear relation between the variables are described. These methods are then applied to indicate the likelihood of a relation between the changes in different parameters. A first example is given with a correlation analysis between the dune parameters in Section 7.2. Furthermore, possible relationships with meteorology (Section 7.3) and tides (Section 7.4) are described. These phenomena are chosen, because bed forms in seas and estuaries can be influenced due to storm-driven and tidal currents [1], [26]. Therefore, it is interesting to investigate the influence of changes in these effects on the subaqueous sand dunes in the Scheldt estuary.

7.1 Correlation analysis

The two methods used to investigate whether there exists a relationship are *correlation coefficient analysis* and *principal component analysis*. These techniques give insight in the strength of a possible linear connection between different variables.

7.1.1 Correlation coefficient analysis

One way to look at the strength of the linear relationship is by calculating the correlation coefficient. This correlation coefficient is much easier to interpret than the covariance and reads [4]:

$$\rho_{ij} = \frac{\sigma_{ij}}{\sigma_i \sigma_j} \tag{7.1}$$

Hence, the correlation coefficient is nothing more than a scaled covariance. It provides only a measure for the linear relation between variables. It quantifies the quality of a least squares linear fit through the original data and is therefore strongly affected by extreme values. The range of the correlation coefficients lies between -1 and 1. An outcome of -1 represents a perfect

negative correlation, a coefficient which equals 0 indicates a total lack of correlation and a perfect positive correlation has the value 1. One must keep in mind that two complete random variables usually have a small correlation coefficient, i.e. its value does not get a clear meaning until the outcome is rather large.

7.1.2 Principal component analysis

A related way to investigate possible correlation is by using the method of Principal components. Principal component analysis (PCA) involves a mathematical operation that transforms the correlated dataset into a number of uncorrelated factors, called *principal components*. The first principal component accounts for the maximal part of the total variance of the variables. Each succeeding component extracts as much of the remaining variability as possible. The results of this transformation can be used for various objectives, like data compression and multivariate outliers detection. A third important application is the possibility to detect linear correlation [25].

In the following we derive the matrix which transforms the original variables into uncorrelated factors [25]:

Let Z be a $n \times N$ matrix of data from which the means of the data have already been subtracted. Here, n is the number of samples and N the number of factors. The corresponding experimental variance-covariance matrix V reads:

$$V = \frac{1}{n} Z^T Z \tag{7.2}$$

Y is a matrix of the same size as Z. The variance-covariance matrix D then reads:

$$D = \frac{1}{n} Y^T Y \tag{7.3}$$

We are looking for an orthogonal matrix A, which linearly transforms the measured variables Z into synthetic factors Y:

$$Y = ZA \quad \text{with } A^T A = I. \tag{7.4}$$

Multiplying from the left by $\frac{1}{n} Y^T$ leads to

$$\frac{1}{n} Y^T Y = \frac{1}{n} Y^T ZA. \tag{7.5}$$

As $Y = ZA$, the equation can be written as

$$\frac{1}{n} Y^T Y = \frac{1}{n} (ZA)^T (ZA) = \frac{1}{n} A^T Z^T ZA = A^T \frac{1}{n} (Z^T Z) A \tag{7.6}$$

and by replacing $\frac{1}{n} Y^T Y$ by D and $\frac{1}{n} Z^T Z$ by V, it follows

$$D = A^T V A \tag{7.7}$$

and consequently

$$VA = AD \tag{7.8}$$

This is nothing else than an eigenvalue problem, as it can be seen as the following equation:

$$VQ = Q\Lambda \quad \text{with } Q^T Q = I \tag{7.9}$$

with Q the matrix of orthonormal eigenvectors of V.

Hence, the orthonormal eigenvectors of V offer the solution to this problem. The matrix of these eigenvectors can transform the measured data into the uncorrelated factors and thus forms the matrix A. The eigenvalues Λ are then the variances of the factors Y.

The principal component analysis allows us to define a sequence of orthogonal factors which absorb a maximal amount of the variance of the data. The eigenvalues indicate the amount of the total variance associated with each factor (see for proof [25]). This transformation enables one to compress data by only taking into account a number of components with the largest variances. On the other hand, if a linear relation is assumed between two datasets, a PCA can indicate the strength of this relation by calculating the variance of the first principal component. The variance, expressed in % of the total variance, tells us the importance of this factor. A large percentage indicates a strong correlation, as in that case a large part of the data can be described using only one principal component.

The correlation between the principal components and the variables can be represented in a *circle of correlation*. The circle of correlations shows the proximity of the variables inside a unit circle and is useful to evaluate the affinities and antagonisms between the variables [25]. The position of the variables on the circle are determined by the correlation coefficient between the variable and the first principal component (x-coordinate) and the second principal component (y-coordinate). These circles give a clear overview of possible correlations.

7.2 Correlation of the classification results

Visually, the results from the classification process in Chapter 4 seem to show a correlation between the dune parameter values. The areas having a small amplitude, do also have a small wave length. From the literature, it is known that in some areas a strong correlation between the wave length, amplitude and depth is observed [3], [20]. Therefore, it is interesting to investigate if and how strong correlation between the parameter values in this part of the Western Scheldt can be found.

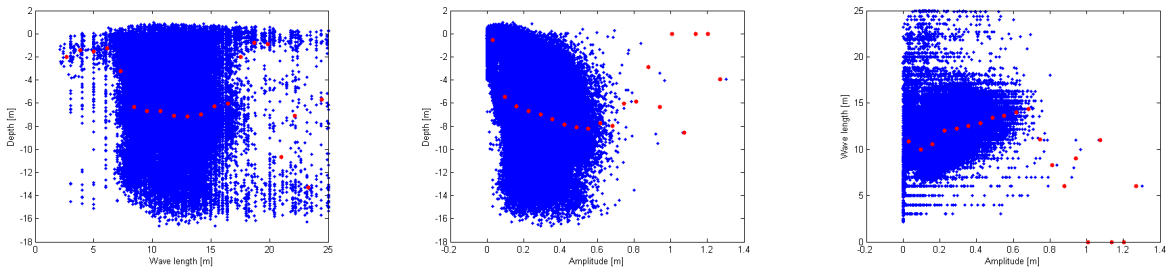

Figure 7.1: The scattergrams between the wave length and depth (left), the wave length and amplitude (center) and between the amplitude and depth (right).

Visual inspection

A first impression can be obtained by plotting the three different components, depth, amplitude and wave length, against each other in three scattergrams, shown in Figure 7.1. These point clouds look rather indistinct and to get insight in the plots, the same procedure is used as in the common experimental variogram procedure, dividing one axis in intervals and calculating the mean of all the points within this set. Clearly one can see a linear trend in the depth-amplitude and in the amplitude-wave length plots. However, the results of the depth-wave length relation is in contradiction with the former two. One way to get insight in this problem is to look at the strengths of the relation by calculating the principal components and the correlation coefficients.

Mathematical correlation analysis

The results for the correlation coefficients can be found in Table 7.1 and for the Principal Component Analysis in Table 7.2. The correlation coefficient results do not show clear linear relations, only the result between the amplitude and the wave length indicate a possible, but weak, correlation. In the other relations, the correlation coefficient is extremely low. This indicates a total lack of correlation. Table 7.2 gives the percentage of the variance used in the first principal

	Wave length	*Amplitude*	*Depth*
Wave length	1.00	0.41	-0.06
Amplitude	0.41	1.00	-0.20
Depth	-0.06	-0.20	1.00

Table 7.1: Correlation coefficients for the relations between the wave length, amplitude and depth.

component. One can see there seems to be a relation, however not very strong, between the wave length and amplitude. In the other two cases, the first component is not significantly different from the second, which means that the correlation is very weak. A visualization can be made by calculating the correlation between the first two principle components and the variables. This correlation is shown in a circle of correlation, which can be seen in Figure 7.2. The appearance of variables closely to each other can indicate a relation. This is visible in the circle, where the amplitude and wave length are closely projected to each other. The results of the two mathematical techniques indicate the same information, which is logical as they are closely related.

	Wave length	*Amplitude*	*Depth*
Wave length	100	70	53
Amplitude	70	100	60
Depth	53	60	100

Table 7.2: Variance in % of the first principal components by the correlation analysis between the wave length, amplitude and depth.

Hence, a possible relation between the amplitude and wave length is observed with the three techniques, visual inspection, principal components and correlation coefficients. The reason for the rather small correlation outcome may be found in the disturbances of the classification method indicated in Section 4.1.3.

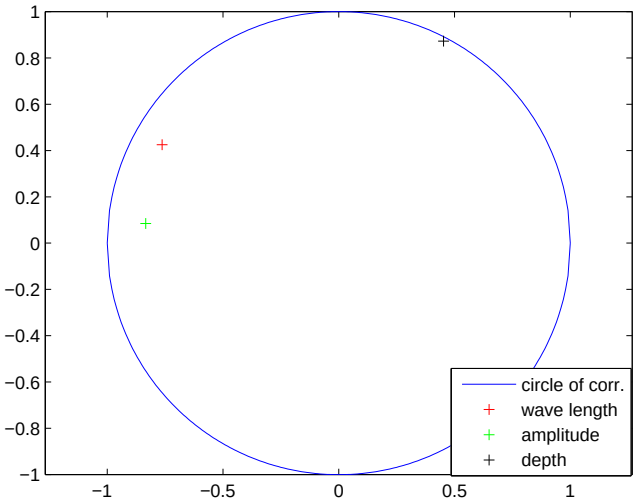

Figure 7.2: The position of the amplitude, wave length and depth inside the circle of correlations for the first two principle components.

7.3 Correlation meteorological data

In order to understand the changes in the morphological parameter values, the obtained amplitude and wave length are linked with meteorological data. It is investigated whether the changes in the estuary bed can be explained from the weather conditions. This study is be performed with a visual inspection and the two mathematical methods: correlation coefficient analysis and principal component analysis.

Visual inspection

In this method the data is analyzed visually. Therefore, the changes in the parameter values have to be selected. The abrupt changes are of special interest, as these distortions are possibly caused by short term extreme weather conditions. Hence, a first step is to detect unexpected and abrupt parameter value changes.

As can be seen in Figure 7.3, the amplitude dropped abruptly at $t = 29$ in Area B. At this epoch a change in wave length can be noticed as well. It is not visible in Area A because at that epoch the sand dump was taking place. Furthermore, a small sudden change in the parameter values is found at $t = 124$ days (Area B) and $t = 130$ days (Area A). These sudden changes in parameter values are of interest for a comparison with the meteorological data. In order to analyze whether or not there may be some relation between these abrupt changes and the meteorological data, one must investigate the weather conditions.

In Section 2.3 the obtained data parameters from the weather station in Vlissingen [9] are mentioned. For this correlation analysis it is assumed that the maximal wind speed and the precipitation may cause the parameter changes. Therefore, these two parameters are analyzed. In Figure 7.4 one can see the maximum hourly mean windspeed over time and the amount of daily precipitation in the sounding period. The extreme values considering the windspeed

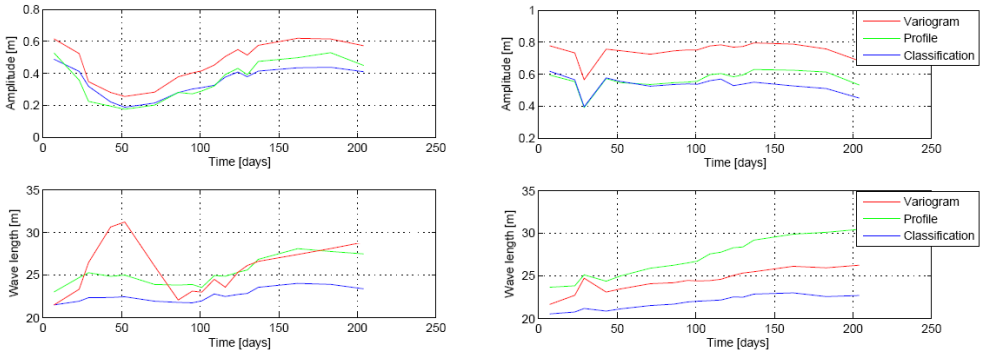

Figure 7.3: The amplitude and wave length as a function of the time for Area A (left) and Area B (right).

happen at day numbers 18, 53, 69, 81, 102, 104, 131, 137, 158. A lot of precipitation occurs at day 18 and 102. Thus, the most extreme weather days in between the sounding period are day 18 and day 102.

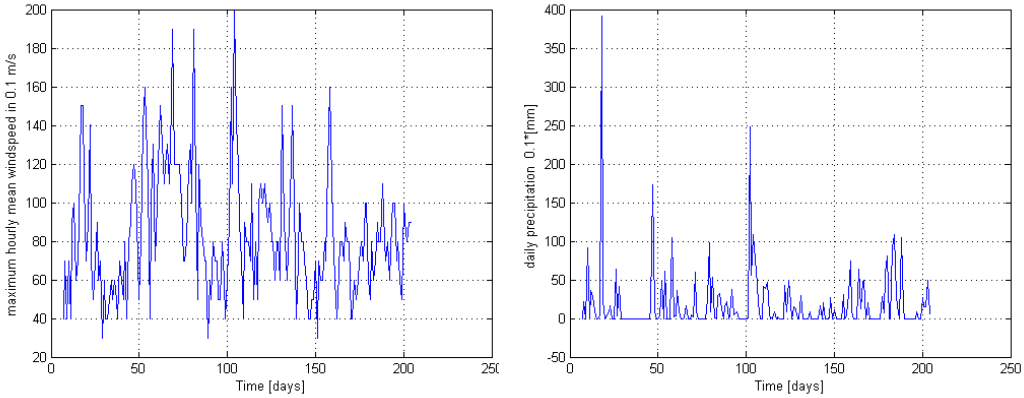

Figure 7.4: maximum hourly mean windspeed in 0.1 m/s (left) and the daily precipitation amount in 0.1 mm (right).

The abrupt morphological changes occur at day numbers 29 and 124 or 130. As the cause of the morphological parameters may be found in the period between the consecutive soundings, the range of time moments $t = [23, 29]$, $t = [116, 124]$ and $t = [124, 130]$ need to be taken into account. However, by visual inspection of the meteorological data no direct relation between the extreme weather and the abrupt morphological changes can be found. Figure 7.5 shows the weather conditions with the outlined parts the time span in which the morphological parameters changed. It can clearly be seen that there is no direct link at these moments.

A second method to visualize possible correlation is by making scattergrams. Here, the morphological changes in between two successive sounding moments are plotted against the highest value of the windspeed and precipitation in between these moments. In Figure 7.6 one can see the results. As the scattergrams do not show a clear pattern, it indicates a lack of correlation.

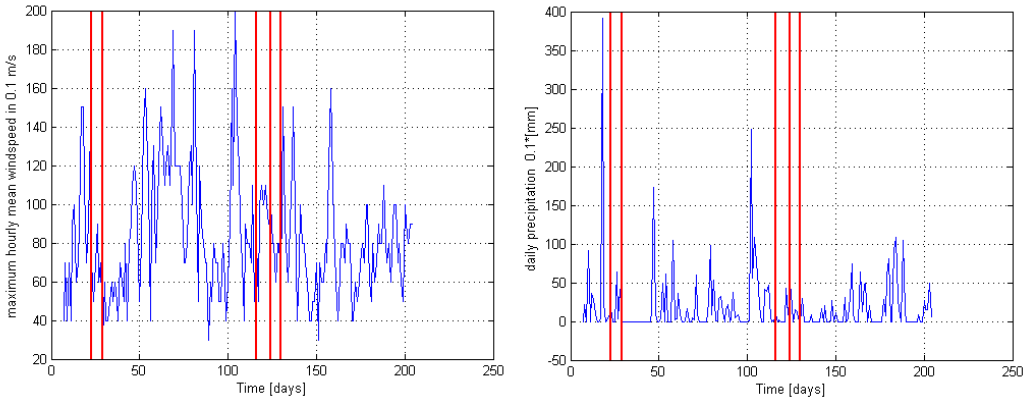

Figure 7.5: maximum hourly mean windspeed in 0.1 m/s (left) and the daily precipitation amount in 0.1 mm (right) with outlined the time span in which the morphological parameters changed.

Mathematical correlation analysis

A possible relation between the parameter changes and the meteorological data can be investigated in a more objective way by the calculation of the correlation coefficients and the principal components. Here, only the obtained parameters from Area B are taken into account, as the others are influenced by the sand dump.

The correlation coefficients between on one hand the maximal precipitation and the wind speed and on the other hand the amplitude and wave length changes are calculated. These coefficients are shown in Table 7.3 and are extremely small, which denotes again an absence of correlation. A correlation analysis by computing the principal components is performed as well. The

	Wave length	*Amplitude*
Wind speed	0.17	-0.031
Precipitation	-0.02	-0.26

Table 7.3: Correlation coefficients of the morphological parameter value changes and the weather conditions.

variance of the first principal factor indicates the strength of a relationship between these two variables. If this value is large, the two parameters can be described by almost one component, which indicates a strong relation. The percentages of the first principal components are shown in Table 7.4. As one can clearly see the variances of the first components is not very large. Therefore, this test indicates that no obvious linear relation between the weather conditions and morphological parameter changes exists. This can also be seen in Figure 7.9, which shows the circle of correlations. The positions of the changes in weather, amplitude and wave length are completely different, which indicates a lack of linear correlation.

All the methods give the same result. A clear relation between the amplitude and wave length changes and the meteorological data can not be found by a mathematical analysis, nor by visual inspection. This does not mean that there is a total lack of correlation between the meteorological data and morphology. For instance, the weather conditions were not that ‘extreme’, the wind

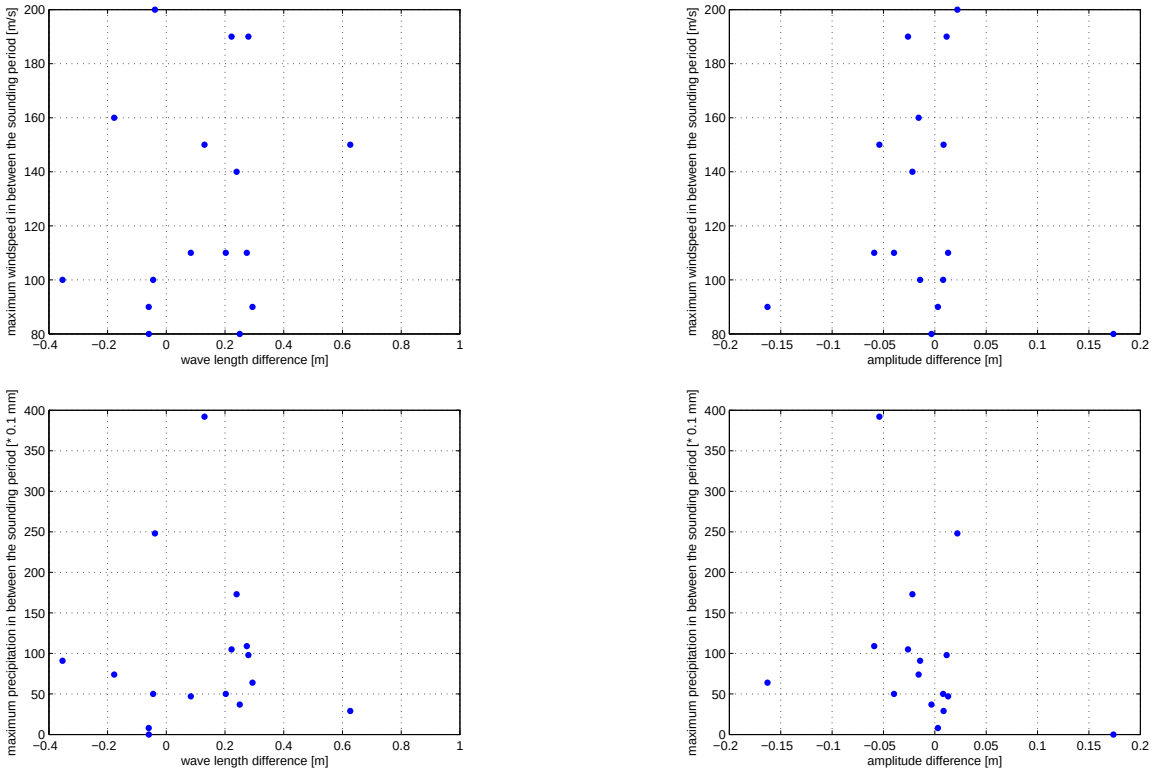

Figure 7.6: Scattergrams between wind speed and amplitude difference (upper left), precipitation and amplitude difference (upper right), wind speed and wave length difference (lower left) and precipitation and wave length difference (lower right).

	Wave length	*Amplitude*
Wind speed	59	52
Precipitation	51	63

Table 7.4: Variance in % of the first principal components by the correlation analysis between morphological changes and the weather conditions.

speed did not reach the storm level in the sounding period. There may still exists a relationship between sand dune parameter values and storm conditions. However, one can conclude that it is not very likely that the abrupt changes in the amplitude and wave length values can be explained from the weather conditions during the sounding moments.

7.4 Correlation tidal information

As no clear correlation between the weather conditions and morphological parameter value changes are found, it is interesting to look further for explanations of the morphological changes. The currents in the Scheldt estuary are tidal-driven and as these currents cause sand dunes, it is investigated whether tidal changes and morphological changes show some correlation.

Visual inspection

The water level is measured near the shoal of Walsoorden. By the correlation analysis on the basis of visual inspections one has to concentrate on some abrupt changes in the morphological parameters, which occur in the intervals $t = [23, 29]$, $t = [116, 124]$ and $t = [124, 130]$. A visualization of the tide, shown in Figure 7.7, does not indicate a direct relation as in these intervals no strange values occur.

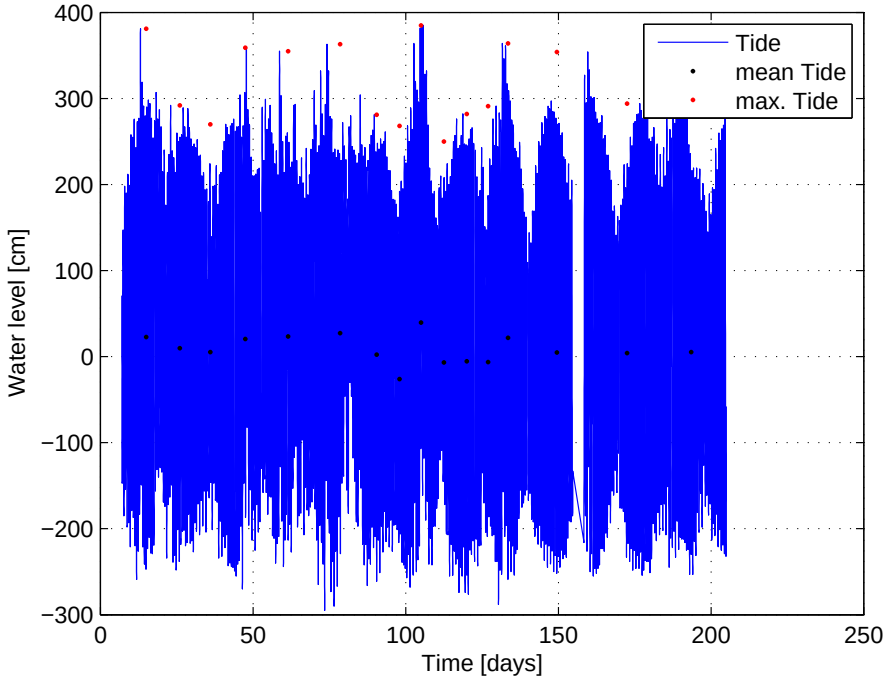

Figure 7.7: The tide during the MBES measurements near the shoal of Walsoorden. The mean and maximal tide are obtained by dividing the data in the same intervals as the sounding moments.

The second method for visual inspection is based on drawing the scattergrams. The mean and maximal values of the tide in between the sounding moments are plotted against the changes in morphological parameters (Figure 7.8). In these scattergrams the plotted points seem rather randomly distributed. No clear trend can be seen, which suggests an absence of linear correlation between the tidal data and morphological parameter value changes.

Mathematical correlation analysis

The correlation between the tidal data and the changes in the sand dunes is also investigated by correlation coefficients analysis and principal component analysis. The correlation coefficient indicate no linear relation at all, as these components are close to zero (Table 7.5). The percentages of the first principal component, shown in Table 7.6 are close to the 50%, which presents the same result.

Figure 7.9 shows the circle of correlations. This plot underlines the results obtained by the

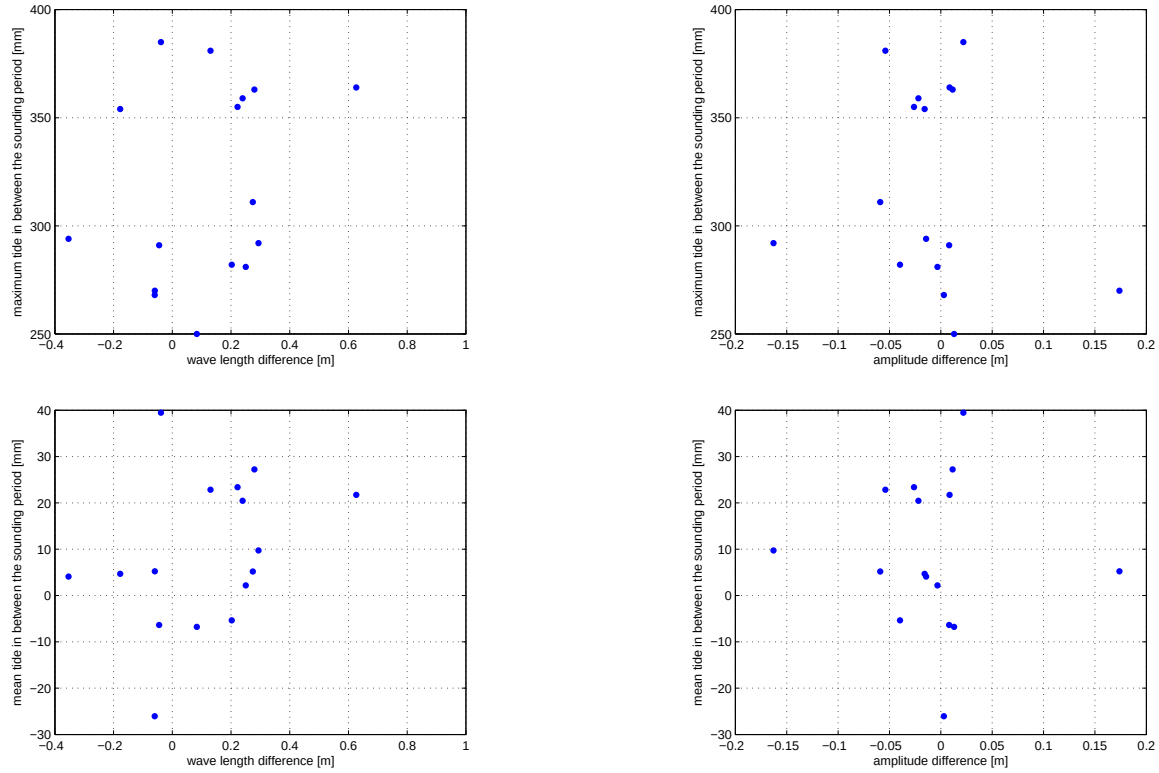

Figure 7.8: Scattergrams between the maximal tide and wave length and amplitude differences (upper plots) and the mean tide and wave length and amplitude differences (lower plots).

	Wave length	*Amplitude*
Maximal tide	0.26	-0.14
Mean tide	0.33	-0.04

Table 7.5: Correlation coefficients of the morphological parameter value changes and the tidal data.

	Wave length	*Amplitude*
Maximal tide	63	57
Mean tide	66	52

Table 7.6: Variance in % of the first principal components by the correlation analysis between morphological changes and the tidal data.

other methods by showing a lack of correlation between the differences in meteorological and tidal data on one hand and the changes in morphological parameters on the other hand. On the other hand, the variables of water level and weather conditions are correlated, as their correlation between its variables and the first two principal components is quite similar. However, the conclusion can be drawn that there is no reason to assume that the morphological changes of the sand dune parameters can be explained or are caused by changes in the maximal tides.

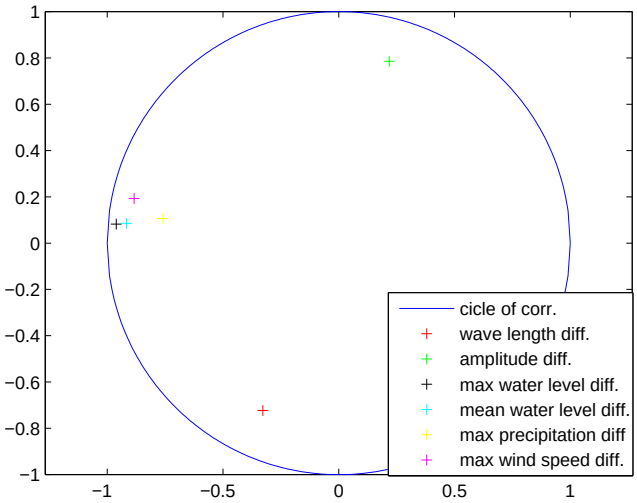

Figure 7.9: The position of the differences in amplitude, wave length, maximal wind speed, maximal precipitation, maximal water level and mean water level inside the circle of correlations for the first two principle components.

Chapter 8

Conclusions and recommendations

As stated in Chapter 1, the objective of this research is to get insight in the complex morphodynamic behaviour of the Western Scheldt bed from a data point of view, using two weekly MBES surveying. The conclusions of this study will be presented in Section 8.1 and a number of recommendations for further research will be done in Section 8.2.

8.1 Conclusions

In order to reach the objective of this study, three research questions are formulated in the introduction. These questions are analyzed for two different cases. First for the analysis of the dump area, where strong changes are expected. Second, a homogeneous and more stable area is selected. The conclusions will be drawn on the basis of these questions, leading to the following three topics:

1. The deformation analysis of the Western Scheldt estuary near the shoal of Walsoorden
2. The morphological parameter changes of the subaqueous bed forms
3. The correlation analysis between the bed forms, weather conditions and tidal data

The deformation of the Western Scheldt

The following conclusions can be drawn from the deformation analysis:

- The separation of the topography and the bed forms provides a good basis for the deformation analysis. The low pass filter results are suitable for the testing of the hypotheses. However, a clear indication of the variance σ^2 which is vital for the calculation of the test statistic $\underline{T}_q$ is difficult to calculate and stays a little indistinct.
- The disposed sand is partly eroding. The deformation analysis shows that almost 75% of the points in the dump region follows the hypothesis of local constant velocity. The points situated in the center and North of the dump area have a negative velocity, which indicates erosion. However, the volume change analysis indicates that most of the disposed sand stays in the region. Only 23% of the dumped material moves out of the disposal area.
- The eroded sand is moving toward the shoal of Walsoorden. The depth of the points south east of the dump location increases over time. As they follow the constant velocity hypothesis with a positive velocity, the conclusion can be drawn that the disposed sand is

transported in this direction. Here, a percentage of about 77% of the moved sand can be found back. The direction agrees with the flood dominating channel orientation near the shoal of Walsoorden. The direction of this movement was an expected effect in this pilot project.

The morphological parameter changes

For the morphological parameter analysis, one can state the following conclusions:

- The residuals of the low pass filter represent the bed forms in a good way. Therefore, it forms a good a necessary basis for the estimation of its parameters.

- The three methods used for parameter estimation give in general the same results. This gives confidence in the methods and the outcome. The variogram method is a good method for the estimation of the morphological parameters. An advantage of the variogram method is the rather objective way the parameters can be estimated. No assumptions have to be made about the definition of local extrema. On the other hand, this method is rather time consuming and the variances of the parameters are difficult to estimate.

- The amplitude of the subaqueous sand dunes is recovered on the dump location after $t = 150$ days. It takes approximately three months after the disposal before the bed forms reaches the same amplitude.

- The wave length at the dump location increases after the disposal. Possibly this is caused by the properties of the dumped sand or the depth of the region.

- The amplitude of the bed forms in the second region (Area B) stays stable over time. An exception has to be made for the amplitude estimation at $t = 29$ days. Here, a sudden drop is noticed which can not yet be explained.

- The wave length of the bed forms in the second region (Area B) increases slightly over time. Despite the fact that the region is rather stable in the deformation analysis, the sand dune parameters are changing.

The correlation analysis

The conclusions drawn from the correlation analysis are:

- A clear correlation between the obvious present morphological changes and the weather or tidal data is not found. No direct link is found between the sudden drop in amplitude and the precipitation, wind speed or water level in this period. Therefore, the abrupt changes in the amplitude and wave length can not be explained by these natural phenomena.

- There may be a relation between the wave length and amplitude. However, the strength of the linear relation between the wave length and amplitude, calculated by the principal component analysis and correlation coefficient analysis, is rather weak. This can be due to the distortions in the classification procedure.

8.2 Recommendations

In this study insight is given in the complex behaviour of the Western Scheldt bed from a data point of view. However, some recommendations can be given for further research:

- In this study a deformation analysis is performed on the filtered data. However, more precise insight may be gained by formulating a hypothesis, which besides the general trend also describes the subaqueous bed form movements over time.
- More insight in the changes of the estuary bed may be gained by taking other attributes into account. For example, a study of bed form asymmetry and dominant currents can confirm the results of the deformation analysis.
- A research about the morphological parameters from a data point of view, combined with a study about the mechanics of sand dunes, taking e.g. the influence of the grain size and the flow velocity into account, may explain some changes in the parameter estimation.
- In this study the separation between the large scale topography and bed forms is performed using a low pass filter. Although this method gives good results, it could generalize the data too much. More sophisticated techniques, like 2-dimensional Fourier analysis may provide better results.

Bibliography

[1] P.A. Carling, A. Radecki-Pawlik, J.J. Williams, B. Rumble, L. Meshkova, P. Bell, and R. Breakspear. The morphodynamics and internal structure of intertidal fine-gravel dunes: Hills Flats, Severn Estuary, UK. *Sedimentary Geology*, 183:159–179, 2006.

[2] C. D. de Jong, G. Lachapelle, S. Skone, and I. A. Elema. *Hydrography.* Delft University Press, Delft, 2003.

[3] F. Francken, S. Wartel, R. Parker, and E. Taveniers. Factors influencing subaqueous dunes in the Scheldt estuary. *Geo-Marine Letters*, 24(1):14–21, 2004.

[4] P. Goovaerts. *Geostatistics for natural resources evaluation.* Oxford University Press, New York, Oxford, 1997.

[5] Y. Gratton and C. Lafleur. Matlab kriging toolbox 6.1. University of Quebec, 2001. http://www.insr-eae.uquebec.ca/activites/repertoire/profs/yg/krig.htm.

[6] N. Hennis. Automatic outlier detection in multibeam data. Master's thesis, Delft University of Technology, Department of Geodesy, 2003.

[7] A.K. Jain. *Fundamentals of digital image processing.* Prentice-Hall, Inc., New Jersey, 1989.

[8] M.C.J.L. Jeuken. *On the morphological behaviour of tidal channels in the Westerschelde estuary.* PhD thesis, Utrecht University, 2000.

[9] Royal Netherlands Meteorological Institute (KNMI). Daily weather data of the Netherlands, 2001-2007. http://www.knmi.nl/klimatologie/daggegevens/download.cgi?language=eng.

[10] E. Kreyszig. *Advanced engineering mathematics.* Wiley, ninth edition, 2006.

[11] K. Lange. *Numerical analysis for staticians.* Springer, New York, 1999.

[12] E. Leys, Y. Plancke, and S. Ides. Shallow - shallower - shallowest, morphological monitoring Walsoorden. In *Proceedings Hydro '06*, Antwerpen, Belgium, 2006.

[13] T.M. Lillesand and R.W. Kiefer. *Remote sensing and image interpretation.* Wiley, New York, fourth edition, 2000.

[14] R.C. Lindenbergh, T.A.G.P. van Dijk, and P.J.P. Egberts. Separating bedforms of different scales in echo sounding data. In *Proceedings 5th international conference on coastal dynamics 2005*, Barcelona, 2006.

[15] X. Lurton. *An introduction to underwater acoustics.* Springer, 2002.

[16] P. Menting. Detection and prediction of sea floor dynamics. Master's thesis, Delft University of Technology, Department of Geodesy, 2004.

[17] Ministry of Transport, Public Works and Watermanagement. Directorate-General for Public Works and Watermanagement (Rijkswaterstaat). Tidal data near the shoal of Walsoorden, 2004-2005. http://www.hmcz.nl.

[18] J. Polman and M.A. Salzmann. *Handleiding voor de technische werkzaamheden van het Kadaster*. Kadaster, Apeldoorn, 1996.

[19] M.J. Pyrcz and C.V. Deutsch. The whole story on the hole effect. *Newsl. Geostat. Assoc. Australas*, 18:3–5, 2003.

[20] A. Robert. *River processes, An introduction to fluvial dynamics*. Arnold, London, 2003.

[21] P. Sistermans and O. Nieuwenhuis. Case study: Western Scheldt estuary (The Netherlands). Technical report, Eurosion, 2007.

[22] P. J. G. Teunissen. *Adjustment theory*. Delft University Press, Delft, 2000.

[23] P. J. G. Teunissen. *Testing theory*. Delft University Press, Delft, 2000.

[24] H. M. E. Verhoef. Geodetische deformatie analyse, 1997. Lecture notes, Delft University of Technology, Faculty of Geodetic Engineering, in Dutch.

[25] H. Wackernagel. *Multivariate geostatistics*. Springer, Berlin, third edition, 2003.

[26] M. Walgreen, D. Calvete, and H.E. de Swart. Growth of large-scale bed forms due to storm-driven and tidal currents: a model approach. *Continental shelf research*, 22:2777–2793, 2002.